ADVANCING EARTH AND SPACE SCIENCES

JGR Solid Earth

RESEARCH ARTICLE
10.1029/2024JB030293

Consistency Between the Slip History Implied by in Situ ^{36}Cl Exposure Dating on an Active Normal Fault and the Timing of Holocene Coastal Notch Formation, Central Greece

Jenni Robertson[1], Claudia Sgambato[1], Gerald Roberts[1], Zoe Mildon[2], Joanna Faure Walker[3], Francesco Iezzi[4], Sam Mitchell[1], Athanassios Ganas[5], Ioannis Papanikolaou[6], Elias Rugen[7], Varvara Tsironi[5], Joakim Beck[8], Silke Mechernich[9], Georgios Deligiannakis[6], Steve Binnie[10], Tibor Dunai[10], and Klaus Reicherter[11]

[1]School of Natural Sciences, Birkbeck, University of London, London, UK, [2]School of Geography, Earth and Environmental Sciences, University of Plymouth, Plymouth, UK, [3]Institute for Risk and Disaster Reduction, University College London, London, UK, [4]Department of Earth, Environment and Resources Sciences, University Federico II of Naples, Naples, Italy, [5]Institute of Geodynamics, National Observatory of Athens, Athens, Greece, [6]Natural Resources and Agricultural Engineering, University of Athens, Athens, Greece, [7]Department of Earth Sciences, University College London, London, UK, [8]Centre for Integrative Petroleum Research, King Fahd University of Petroleum and Minerals, Dhahran, Kingdom of Saudi Arabia, [9]Department of Remote Sensing, Federal Institute of Hydrology, Koblenz, Germany, [10]Institute for Geology and Mineralogy, University of Cologne, Cologne, Germany, [11]Institute for Neotectonics and Natural Hazards, RWTH Aachen University, Aachen, Germany

Key Points:

- Spatial pattern of radiocarbon dated deformed Holocene notches agree with the slip implied by ^{36}Cl Pisia fault scarp dating
- N. Perachora Holocene notch elevations explained by 2.0 ka-present day slip on Pisia-Skinos faults and 5.2–2.0 ka slip on Strava fault
- The sub-parallel Pisia and Strava faults are suggested to slip out of phase to one another

Supporting Information:

Supporting Information may be found in the online version of this article.

Correspondence to:

J. Robertson,
j.robertson@bbk.ac.uk

Citation:

Robertson, J., Sgambato, C., Roberts, G., Mildon, Z., Faure Walker, J., Iezzi, F., et al. (2025). Consistency between the slip history implied by in situ ^{36}Cl exposure dating on an active normal fault and the timing of Holocene coastal notch formation, central Greece. *Journal of Geophysical Research: Solid Earth*, *130*, e2024JB030293. https://doi.org/10.1029/2024JB030293

Received 6 SEP 2024
Accepted 20 SEP 2025

Author Contributions:

Conceptualization: Jenni Robertson, Gerald Roberts
Formal analysis: Jenni Robertson
Funding acquisition: Jenni Robertson, Gerald Roberts
Investigation: Jenni Robertson, Claudia Sgambato, Gerald Roberts, Zoe Mildon, Joanna Faure Walker, Francesco Iezzi, Sam Mitchell, Athanassios Ganas, Ioannis Papanikolaou, Elias Rugen, Varvara Tsironi
Methodology: Jenni Robertson, Claudia Sgambato, Gerald Roberts, Joakim Beck

Abstract We report agreement between the timing of slip on an active normal fault recovered from in situ ^{36}Cl cosmogenic fault scarp dating with independently ^{14}C dated Holocene coastal notches deformed along the strike of the fault, reinforcing the validity of slip-rate timing and magnitude fluctuations implied by ^{36}Cl fault scarp dating. The ^{36}Cl-dated Pisia fault, central Greece, shows slip-rate fluctuations but the timing of slip derived from this cosmogenic isotope have not been confirmed with an independent dating approach. However, Holocene coastal notches dated with ^{14}C on fossils occupying the notches exist around the Pisia fault, these can only form when the interplay between eustatic sea-level and tectonics result in stable relative sea-level. The ^{36}Cl site close to the center of the Pisia fault records ongoing slip from ~9.6 to 5.2 (±0.5) ka and 2.0 ± 0.5 ka to the present day which was interrupted by a low slip-rate period. Holocene sea-level stabilized close to its current elevation after 7.0–6.5 ka, so the combination of low slip-rate and stable sea-level allowed notch formation. During this time, notches were uplifted by slip on the offshore Strava fault, indicated by elastic half-space modeling. Toward the center of the Pisia-Skinos fault, these notches were then submerged during the high slip period from 2.0 ± 0.5 ka. Our findings reveal that spatial patterns of deformed radiocarbon-dated Holocene notches agree with the timing of high slip earthquake clusters/quiescent anti-clusters from ^{36}Cl slip histories and support use of ^{36}Cl to investigate normal faults, crustal rheologies and seismic hazard.

Plain Language Summary Changes in the slip rates on normal faults through time can be investigated using concentrations of the cosmogenic isotope ^{36}Cl measured from fault scarps. These ^{36}Cl concentrations can be numerically modeled to derive the history of earthquake slip on the fault. We show agreement between the histories of earthquake slip on the Pisia fault (central Greece) from ^{36}Cl fault scarp dating when compared to another independent dating technique (^{14}C) carried out on fossils that grew along the coastline in coastal notches when the Pisia fault was not slipping between 5.2 ± 0.5 ka and 2.0 ± 0.5 ka and when sea level was stable. We find that the present-day elevations of the coastal notches, which vary along the coastline from being exposed above sea level to submerged below sea level, is consistent with alternating fault activity on the Pisia fault and on the Strava fault which is located sub-parallel to the Pisia fault. Our study is important because the consistency between slip rate changes implied by ^{36}Cl fault scarp dating and independent notch age controls emphasizes that ^{36}Cl on fault scarps can be used to inform our understanding of the hazards posed by normal faults and how continents deform.

1. Introduction

In situ ^{36}Cl cosmogenic exposure dating on fault scarps has enhanced our ability to investigate the slip accommodated on normal faults because it provides insight into their temporal slip histories over tens of thousands of

Project administration: Jenni Robertson, Gerald Roberts
Resources: Silke Mechernich, Georgios Deligiannakis, Steve Binnie, Tibor Dunai, Klaus Reicherter
Software: Joakim Beck
Supervision: Gerald Roberts
Visualization: Jenni Robertson
Writing – original draft: Jenni Robertson
Writing – review & editing: Claudia Sgambato, Gerald Roberts, Zoe Mildon, Joanna Faure Walker, Francesco Iezzi, Sam Mitchell, Athanassios Ganas, Ioannis Papanikolaou, Elias Rugen, Joakim Beck, Silke Mechernich, Georgios Deligiannakis, Steve Binnie, Tibor Dunai, Klaus Reicherter

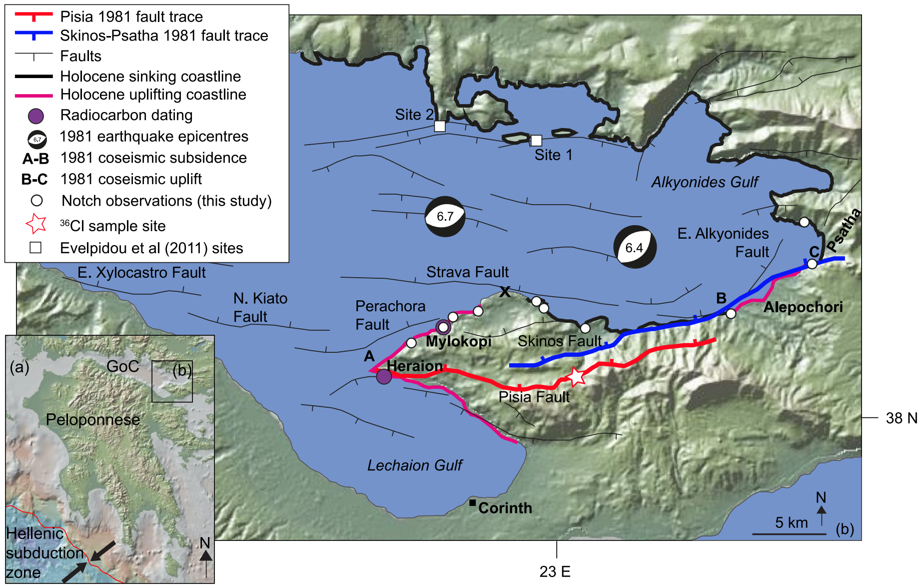

Figure 1. (a) Location of the Gulf of Corinth. (b) Eastern Gulf of Corinth and the Perachora Peninsula. Epicenters of the 24th and 25th February 1981 earthquakes (relocated from Jackson et al. (1982) by Taymaz et al. (1991)). Pisia and Skinos-Psatha fault traces from 1981 ruptures (Hubert et al., 1996; Jackson et al., 1982; Roberts, 1996a). Offshore faults as per Nixon et al. (2016). ^{36}Cl sample site from Mechernich et al. (2018). Locations of age controls from radiocarbon dating of fossils removed from notches (Pirazzoli et al., 1994). Uplifting and subsiding coastlines marked on the map are from Jackson et al. (1982). Also included are the locations of submerged notches observed on the coastline of the north Alkyonides Gulf (Evelpidou et al., 2011). "X" marks the location of no observed subaerial notches and suspected submerged notches (see text for detail).

years (Benedetti et al., 2002, 2003, 2013; Dawood et al., 2024; Iezzi et al., 2021; Mechernich et al., 2018, 2023; Mildon et al., 2022; Mozafari et al., 2019, 2021; Palumbo et al., 2004; Roberts et al., 2024, 2025; Tesson & Benedetti, 2019; Zreda & Noller, 1998). However, fault slip histories obtained from in situ ^{36}Cl exposure dating on fault scarps are commonly published without support from other independent age controls associated with Holocene faulting activity. Paleoseismic trenching studies located near to ^{36}Cl exposure fault plane sampling sites may offer the opportunity to calibrate the ages associated with slip-rate histories derived from ^{36}Cl, but may be limited by the duration of time constrained by dating of materials in the trench. Validating in situ ^{36}Cl cosmogenic exposure dating on fault scarps is important because such studies contribute to our understanding of temporal earthquake behavior. Specifically, results from ^{36}Cl suggest that active normal faults exhibit episodic behavior with alternating clusters of earthquakes resulting in periods of rapid slip that are separated by periods of relatively slow slip or even quiescence. Such insights are facilitating greater understanding into the causal mechanisms associated with earthquake clustering, the stress interaction between neighboring faults and their ductile shear zones at depth and, that decadal geodetic rates of extension may differ from rates over longer timescales (e.g., Iezzi et al., 2021; Mildon et al., 2022; Roberts et al., 2024, 2025; Sgambato et al., 2025). Thus, the findings from studies that employ ^{36}Cl exposure dating on fault scarps have the capacity to improve how we address seismic hazard assessment associated with normal faults.

To consider the slip histories derived from ^{36}Cl exposure fault scarp dating in the context of other geomorphic evidence of faulting, we have identified a location on the Perachora Peninsula in central Greece, where deformed Holocene coastal notches hosting fossils have been dated with ^{14}C (Figure 1). The coastline is predominantly located in the hanging wall of the Pisia and Skinos normal faults which form part of the ~40 km-long South Alkyonides Fault System (SAFS) (Leeder et al., 2005; Morewood & Roberts, 1997, 1999, 2001, 2002; Roberts, 1996a; Roberts et al., 2009). Recent ^{36}Cl exposure dating on the Pisia fault attests to earthquake slip throughout the Holocene with fluctuating slip-rates, stated to be as low as 0.37 mm/yr and as high as 2.3 mm/yr (Mechernich et al., 2018). Along parts of the north Perachora coastline, Holocene palaeoshorelines in the form of marine notches are evident in the carbonate rocks that bound the coastline (e.g., Evelpidou et al., 2023; Jackson et al., 1982; Kershaw & Guo, 2001; Pirazzoli et al., 1994; Schneiderwind, Boulton, Papanikolaou, &

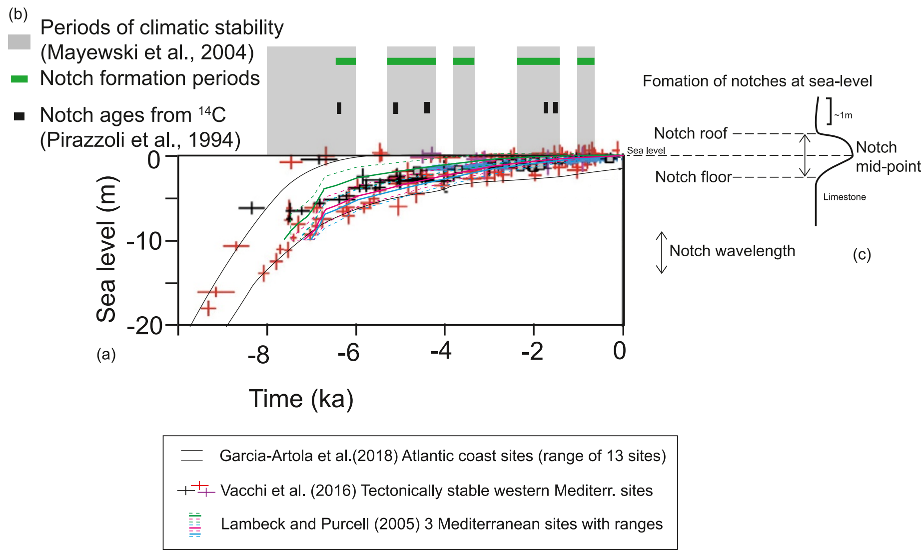

Figure 2. (a) Holocene sea-level reconstructions reproduced from Garcia-Artola et al. (2018), Lambeck and Purcell (2005) and Vacchi et al. (2016). (b) Age controls from Pirazzoli et al. (1994) plotted against periods of climatic stability (Mayewski et al., 2004) which are suggested to act as a proxy for Holocene sea-level stability (Cooper et al., 2007). Green bars in (b) indicate when notches are hypothesized to form during periods of Holocene climate/sea-level stability as per Cooper et al. (2007). (c) Schematic diagram of a notch and where notch elevation measurements were made.

Reicherter, 2017, Schneiderwind, Boulton, Papanikolaou, Kázmér, & Reicherter, 2017). These palaeoshorelines are particularly important because radiocarbon (^{14}C) dating on fossils encrusting the notches and that have been removed from borings into the limestone implies the timing of notch formation in the Holocene (Pirazzoli et al., 1994). Specifically, at two localities close to the western tip of the Pisia fault, two sequences of subaerial notches in the footwall and hanging wall were dated by Pirazzoli et al. (1994) (Figure 1) which suggest five distinct fossil growth ages between 6,434 and 6,314 years BP, 5,164–5,004 years BP, 4,434–4,254 years BP, 1,804–1,554 years BP and 1,594–1,454 years BP, with a sixth age discounted by the authors (Pirazzoli et al., 1994) (Figure 2a). Note that these growth ages take into account that radiocarbon ages can be 350–400 years older than their real age because of the incorporation of host-rock carbon (Evelpidou, Vassilopoulos, & Pirazzoli, 2012). Whilst studies have shown that older Holocene notches can be overprinted by notches associated with younger relative sea-level change (Faivre et al., 2021; Schneiderwind, Boulton, Papanikolaou, & Reicherter, 2017) we note that the radiocarbon age controls from Pirazzoli et al. (1994) from the north Perachora coastline implies increasing notch age with elevation.

Studies investigating Holocene sea-level elevations in the Mediterranean imply that notches are not expected to have formed prior to 7.0–6.5 ka. This because following the demise of the Last Glacial Maximum (LGM) rapid sea level rise occurred until 7.0–6.5 ka, after which sea-level rise slowed and stabilized. Such insight comes from sea-level reconstructions (e.g., Garcia-Artola et al., 2018; Lambeck & Purcell, 2005; Vacchi et al., 2016) and high-resolution climate proxy records (Mayewski et al., 2004), and is in agreement with age controls on Holocene notches (Boulton & Stewart, 2015; Cooper et al., 2007; Pirazzoli, 1991; Pirazzoli et al., 1994; Schneiderwind, Boulton, Papanikolaou, Kázmér, & Reicherter, 2017) (Figure 2).

In this study we aim to link observations made on subaerial and submerged Holocene notches along the north Perachora coastline with the Holocene slip history from in situ ^{36}Cl cosmogenic exposure fault scarp dating using vertical deformation modeling of earthquakes on the Pisia and Skinos-Psatha faults. We mapped the broad-scale vertical deformation of marine notches over a 30 km east–west transect, measuring the elevations of notches located above and below present-day sea level. We remodel the ^{36}Cl concentrations obtained from the Pisia fault (Mechernich et al., 2018) using a numerical code (Beck et al., 2018) developed since these data were published. The result of this remodeling allows us to link the timing of a 2.0 ± 0.5 ka to present-day recent high-slip period with the spatial pattern of along-strike notch elevations using models of coseismic vertical deformation derived from elastic half-space modeling of earthquakes on the Pisia fault and other faults located along and across strike. Our results show that the timing of notch formation, emergence and subsequent along-strike deformation can be explained by the timing of Holocene earthquake clusters and anti-clusters on the Pisia fault implied by ^{36}Cl exposure dating. These results reinforce the validity of ^{36}Cl exposure dating as a method to derive the multi-millennial slip histories on normal faults because for the first time the timings of rapid and slow slip episodes are shown to agree with age constraints provided by ^{14}C dates for Holocene notches.

2. Background

2.1. Geological Background and Seismicity

The Gulf of Corinth is a rapidly extending basin that accommodates horizontal extension between 5 and 15 mm/yr via numerous faults that predominantly bound the southern coastline of the Gulf (Armijo et al., 1996; Bell et al., 2009; Briole et al., 2000, 2021; Clarke et al., 1998; Davies et al., 1997; Nixon et al., 2016). Our work focuses on the Perachora Peninsula, located in the east of the Gulf, where recent estimates suggest an extension rate of 5.4 mm/yr (Briole et al., 2021). The Perachora Peninsula is a fault bounded horst that separates the Alkyonides Gulf in the north and the Lechaion Gulf in the south (Figure 1) (Charalampakis et al., 2014; Stefatos et al., 2002). The South Alkyonides Fault System (SAFS) extends from the western tip of the Perachora Peninsula and is comprised of four fault segments, from west to east these are the Pisia, Skinos, East Alkyonides and Psatha faults (Morewood & Roberts, 1997, 1999, 2001, 2002; Leeder et al., 2005; Roberts, 1996a; Roberts et al., 2009). A maximum cumulative throw of 2.5 km in the center of the fault system, combined with slip vectors from the onshore Pisia, Skinos and Psatha faults that converge toward the center of the fault system implies that the four fault segments work together as a single overall fault structure (Morewood & Roberts, 1999; Roberts, 1996a, 1996b; Roberts & Ganas, 2000). Whilst the Perachora Peninsula is dominated by the north-dipping SAFS, deformation offshore is accommodated by north and south dipping faults (Figure 1) that are suggested to have been active throughout the Holocene (Ambraseys & Jackson, 1990; Bell et al., 2009; Charalampakis et al., 2014; Nixon et al., 2016; Sakellariou et al., 2007; Stefatos et al., 2002).

In 1981 a sequence of three earthquakes occurred in the eastern Gulf of Corinth on the 24th (Mw 6.7) and 25th (Mw 6.4) February and on the 4th March (Mw 6.4) (Jackson et al., 1982). Debate has centered around which faults ruptured in the 24th and 25th February earthquakes (Abercrombie et al., 1995; Jackson et al., 1982; Kim et al., 1984; Papazachos et al., 1984; Taymaz et al., 1991; Vita-Finzi & King, 1985) (note that the 4th March earthquake occurred on the Kaparelli fault approximately 25 km to the north east, and is not discussed further herein). After detailed analyses of the earthquake source parameters (e.g., Abercrombie et al., 1995; Taymaz et al., 1991) in combination with coastal observations of subsidence and uplift (e.g., Hubert et al., 1996; Khoury et al., 1983; Stiros & Pirazzoli, 1998; Vita-Finzi & King, 1985) it may be that the 24th February earthquake ruptured the Pisia fault, and the 25th February earthquake ruptured the Skinos fault with this latter rupture suggested to have extended eastward along the East Alkyonides and possibly Psatha faults (Figure 1). Coseismic surface ruptures and coastal deformation associated with the February 1981 earthquakes were observed from close to the western tip of the Pisia fault at Heraion toward the Psatha fault (red and blue traces in Figure 1) (Bornovas et al., 1984; Collier et al., 1998; Hubert et al., 1996; Jackson et al., 1982; Khoury et al., 1983; Mitchell et al., 2024; Roberts, 1996a; Roberts et al., 2009; Roberts & Ganas, 2000; Robertson et al., 2020; Vita-Finzi & King, 1985). Coseismic displacement of up to 223 and 130 cm was evident on the limestone free face of the Pisia and Skinos faults, respectively, and in the colluvium or angular scree of the hanging walls of the faults (Jackson et al., 1982; Mitchell et al., 2024; Roberts, 1996a). Evidence of coseismic deformation from slip on the onshore (Pisia, Skinos and Psatha) and offshore (East Alkyonides) faults along the coastline has been associated with the 1981 earthquakes. Specifically, where the coastline is in the hanging wall of the Pisia and Skinos faults subsidence was observed (A-B, Figure 1), whilst coastline uplift occurred in the footwalls of the East Alkyonides and Psatha faults (directly east of B-C, Figure 1) (Hubert et al., 1996; Khoury et al., 1983; In Stiros & Pirazzoli, 1998; Vita-Finzi & King, 1985). Submerged notches on the north of the Gulf of Alkyonides coastline have also been associated with the 1981 earthquake sequence (Evelpidou et al., 2011) (Figure 1). The observed deformation cannot be assigned to individual earthquakes because they occurred so closely spaced in time and space. However, the spatial extent of the February 1981 surface ruptures and coastline observations suggest that rupture occurred on all four segments of the SAFS. Herein, we refer to the Mw 6.7 24th February earthquake as the Pisia earthquake and the Mw 6.4 25th February earthquake as the Skinos-Psatha earthquake (Taymaz et al., 1991).

Uplifted Pleistocene to Holocene palaeoshorelines on the north Perachora coastline points to a spatial pattern of uplift and subsidence that is not consistent with the pattern of reported 1981 coseismic subsidence (Figure 1). In more detail, the presence of subaerial coastal notches was used to demarcate areas of uplifting and sinking coastlines over the Holocene (Jackson et al., 1982; Stewart & Vita-Finzi, 1996) (Figure 1). Specifically, Jackson et al. (1982) observed subaerial Holocene notches over an ∼8 km section of the western north Perachora coastline and in the area east of Alepochori (Figure 1). Where uplifted Holocene notches are observed, Pleistocene palaeoshorelines and their associated marine terraces/erosional wave-cut platforms are also reported (Collier et al., 1992; Dia et al., 1997; Kershaw & Guo, 2003; Leeder et al., 2003, 2005; Morewood & Roberts, 1997, 1999; Robertson et al., 2020). The presence of Holocene and Pleistocene palaeoshorelines along the parts of the north Perachora coastline imply that in some places the dominant motion through time is uplift even though this area experienced coseismic submergence in the 1981 Pisia and Skinos-Psatha earthquakes. Consequently, it is pertinent to highlight the presence of local offshore north-dipping faults that may be responsible for uplift of the north Perachora coastline, namely the Strava and Perachora faults (Figure 1). The Perachora fault (Figure 1) is the eastern most fault of a set of three en-echelon faults (East Xylocastro, North Kiato and Perachora faults) that host a single depocenter in their hanging wall and are suggested to be linked at depth (Armijo et al., 1996; Nixon et al., 2016) (Figure 1). Activity on these offshore faults is indicated by sediments that thicken into the hanging walls (Nixon et al., 2016; Stefatos et al., 2002). The north-dipping Strava fault forms the southern fault of the Strava graben. Numerous seismic reflection surveys investigating the Strava fault evidence stratal thickening implying that the fault has been active throughout the Pleistocene into the Holocene and constrain its location to be ∼1 km north of the northern Perachora coastline (Figure 1), but these studies vary regarding the length of the fault (Bell et al., 2009; Charalampakis et al., 2014; Nixon et al., 2016; Papatheodorou & Ferentinos, 1993; Sakellariou et al., 2007; Stefatos et al., 2002; Taylor et al., 2011).

2.2. Introduction to the Formation and Significance of Marine Notches

Along carbonate coastlines, marine notches form through a combination of physical, biological and chemical processes (e.g., Kershaw & Guo, 2001; Pirazzoli, 1986; Pirazzoli & Evelpidou, 2013; Rust & Kershaw, 2000; Trenhaile, 2015) with their morphology dependent on the dominant process of formation, the lithology and bedrock heterogeneity, local climate and local tectonics (e.g., Evelpidou, 2012; Evelpidou, Kampolis, et al., 2012; Kershaw & Guo, 2001; Schneiderwind, Boulton, Papanikolaou, Kázmér, & Reicherter, 2017). Tidal and biological erosion rates of 0.2–1 mm/yr in the Mediterranean imply that limestone notches could take from a few hundred years up to a thousand years to form (Antonioli et al., 2015; Evelpidou & Pirazzoli, 2016; Pirazzoli & Evelpidou, 2013; Schneiderwind, Boulton, Papanikolaou, & Reicherter, 2017). Previous studies investigating notches in the eastern Gulf of Corinth attest to the complexity of conditions associated with their formation. At Heraion, on the western tip of the Perachora Peninsula (Figure 1), coastlines show variable notch profiles, with four notches evident on the south coast in the footwall of the Pisia fault and two notches evident on the north coast (in the hangingwall of the Pisia fault), just a few hundred meters apart (Kershaw & Guo, 2001; Pirazzoli et al., 1994). Similarly, at Mylokopi (Figure 1), on the north coast, there is variation in the number and elevation of notches over just a few hundred meters (Kershaw & Guo, 2001; Pirazzoli et al., 1994; Schneiderwind, Boulton, Papanikolaou, & Reicherter, 2017), where the west of the bay hosts two notches, a central block hosts between two and four notches and the eastern coastline hosts two notches. Kershaw and Guo (2001) suggest that the Mylokopi notch variations represent the heterogeneous process of notch formation linked to local variations in wave and surf regime, bedrock heterogeneity and localized fault movements. Terrestrial Lidar Scanning (TLS) combined with modeling applied to the Mylokopi notches suggested that repeated Mw 6.7 Holocene events on the offshore north-dipping Strava fault are expected to be responsible for individual uplift events of up to ∼0.4 m (Schneiderwind, Boulton, Papanikolaou, & Reicherter, 2017).

In the Mediterranean, the formation and emergence of Holocene notches has been examined in detail and is associated with the stability of the sea level and coastline (e.g., Boulton & Stewart, 2015; Cooper et al., 2007; Evelpidou et al., 2014; Pirazzoli et al., 1996; Schneiderwind, Boulton, Papanikolaou, Kázmér, & Reicherter, 2017; Stewart & Vita-Finzi, 1996). Notch sequences have been suggested to form because coastline uplift rates match the rates of sea-level rise with discrete coseismic events with magnitudes greater than Mw 6 suggested to be responsible for uplifting a notch above its present-day sea level (e.g., Boulton & Stewart, 2015; Pirazzoli et al., 1996; Trenhaile, 2015). However, detailed coseismic uplift observations following Mw ∼6–7 normal faulting earthquakes challenged this explanation because footwall coseismic uplift is not expected to exceed a few decimeters per event (e.g., Ganas et al., 2021; Papanikolaou et al., 2010; Stein & Barrientos, 1985). Consequently, normal faulting earthquakes that vertically uplift coastlines are not expected to be capable of fully removing a marine notch above the erosional influence of the sea in a single earthquake and instead may result in vertically extending the wavelength of the forming notch (e.g., Schneiderwind, Boulton, Papanikolaou, Kázmér, & Reicherter, 2017).

In the eastern Gulf of Corinth, where normal faulting dominates, it has also been suggested that the formation and emergence of sequences of Holocene notches is linked to the interplay between tectonic motions and periods of regional Holocene climate stability (Cooper et al., 2007). High resolution climatic models that imply oscillation between a rapidly changing and stable climate since ~6.0 ka (Mayewski et al., 2004) were used as a proxy for the stability of Holocene sea levels (Cooper et al., 2007). Cooper et al. (2007) observed that the notch age controls from Pirazzoli et al. (1994) agreed with the timing of stable climatic periods (Mayewski et al., 2004) (e.g., Figure 2a) suggesting that Holocene notch formation may be dependent on both a stable sea level and stable coastline. Another study highlights that using notches to investigate paleoseismicity is complex because they are a regionally variable and diachronous marker (Boulton & Stewart, 2015). In their study, Boulton and Stewart (2015) noted that one of the challenges of the climatic model from Cooper et al. (2007) was that it required uplift rates to be greater than the rate of sea-level rise during times of unstable climate. Overall, although this review has identified key points about notch formation, several un-answered questions remain, such as (a) how notch sequences can be uplifted if single earthquakes cannot lift individual notches out of the marine erosion zone, and (b) how notches can form in locations like the Gulf of Corinth where the existence of active normal faults in the Holocene may hinder the temporal coincidence between stable sea-level and slow coastal uplift.

3. Methods

3.1. Measuring Notch Elevations

In this study we measured the elevations of three morphological features of subaerial (above sea level) or submerged (below sea level) notches: (a) the roof of the notch, (b) the floor of the notch, and (c) the point of maximum horizontal depth of the notch (also known as the vertex and referred to herein as the notch mid-point) (Figure 2c). This latter feature has been suggested to be representative of mean sea level (e.g., Antonioli et al., 2015; Evelpidou et al., 2011; Pirazzoli, 1986). The roof and floor measurements are used to derive the vertical wavelength of a notch. We measured the mid-point, roof and floor elevations of subaerial notches relative to sea level using either a tape measure or a Trupulse Laser where the notch was inaccessible. Submerged notches were measured relative to sea level whilst snorkelling using a surveyor's folding rule on days with fair weather and waves heights of only a few centimeters. We assign ±5 cm errors to measured notch elevations to take into account measurement uncertainties.

We focus on the broad-scale along-strike variations of the spatial patterns of subaerial versus submerged notches. We do not investigate small-scale variations in the number and elevation of notches between individual localities because they are likely to be influenced by local processes such as different site characteristics including wave height, contribution of physical, chemical or biological processes to notch formation, the influence and presence of freshwater springs, and the presence of small-scale faults that intersect the coastline and have resulted in minor offset between adjacent notches (Section 2). We use the radiocarbon ages from Pirazzoli et al. (1994) as indicators that the notches increase in age with elevation, but a lack of ages across the research area and localized faulting where the radiocarbon ages occur in the hangingwall (Section 2) limits the use of these radiocarbon ages in our vertical deformation modeling.

3.2. Re-Modeling ^{36}Cl Concentrations From the Pisia Fault

Samples removed from the surfaces of carbonate fault scarps can be used to derive in situ cosmogenic ^{36}Cl concentrations to investigate slip-rate fluctuations on faults through time (e.g., Benedetti et al., 2002, 2003; Zreda & Noller, 1998). ^{36}Cl accumulates in carbonate rock as it is exposed to the high energy particles that travel through the Earth's atmosphere (Dunai, 2010; Gosse & Phillips, 2001; Schlagenhauf et al., 2010). Earthquake slip exhumes carbonate normal fault planes through a sub-surface ^{36}Cl production zone and as the fault planes emerge from the ground the rate of ^{36}Cl production increases. Consequently, ^{36}Cl concentrations increase up the fault plane because higher sections of the fault plane were exhumed during earlier earthquakes in the slip history and thus have been exposed at the surface for longer. Numerical codes have been developed that use the ^{36}Cl

10.1029/2024JB030293

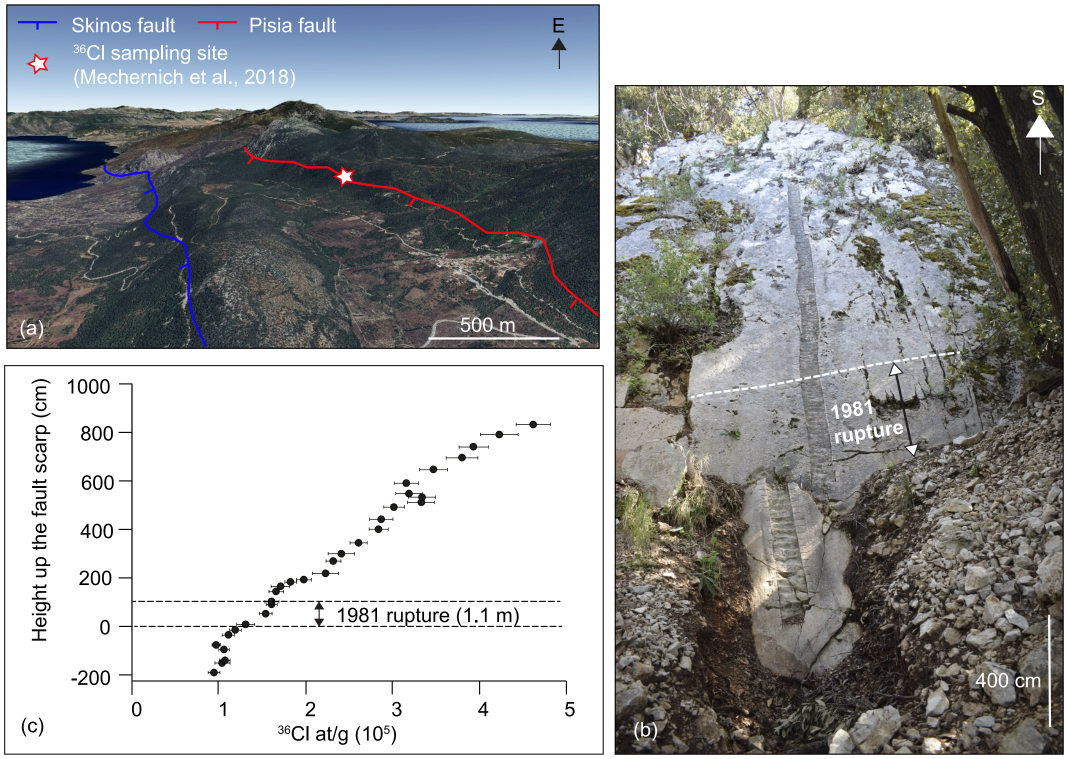

Figure 3. (a) The location of the Pisia ^{36}Cl exposure dating site relative to the trace of the Skinos fault (see also Figure 1), image from Google Earth. (b) Photograph of the ^{36}Cl fault scarp site sampled by Mechernich et al. (2018) with the extent of the 1981 rupture and, (c) a plot of the ^{36}Cl concentrations for samples removed from the Pisia fault scarp published by Mechernich et al. (2018) showing the increase in ^{36}Cl concentrations up the height of the scarp. Also shown is the extent of the 1981 rupture relative to samples removed from the scarp.

concentration data obtained from fault scarps to derive slip histories through replication of the measured ^{36}Cl concentrations (Beck et al., 2018; Cowie et al., 2017; Schlagenhauf et al., 2010; Tesson & Benedetti, 2019; Tikhomirov et al., 2019).

In this study we remodel the ^{36}Cl concentrations from the Pisia fault published by Mechernich et al. (2018) (Figure 3) to derive a slip history using a Bayesian Markov Chain Monte Carlo (MCMC) reverse jump approach developed by Beck et al. (2018). This code carries out several million of slip history iterations on two parallel Markov chains, adopting a forward model approach to reconstruct the ^{36}Cl concentrations by aiming to minimize the misfit between modeled and measured ^{36}Cl concentrations. Slip histories are drawn from a Brownian Passage Time (BPT) earthquake recurrence model that allows both constant and fluctuating slip rates to be tested. Slip histories are considered as acceptable only when the two independent MCMC chains have converged (Beck et al., 2018). The convergence is measured using the Gelman-Rubin diagnostic (Gelman & Rubin, 1992) and requires that the model outputs a Potential Scale Reduction Factor (PSRF) of 1.1 or lower. The output of the inference method includes the posterior distribution of results consisting of the highest likelihood outcomes, the least squares solutions that best fit the data, and also an ensemble of least squares solutions that represent a number of outcomes that best fit the data. The user can then use combinations of these three outcomes to help interpret the results. The Beck et al. (2018) code does not aim to identify the timing of individual earthquakes, instead focusing on periods of high or low slip rate that may imply the presence of temporal clusters or anti-clusters of earthquakes. Periods of high slip rate can be recognized as clusters where the amount of displacement that the fault accommodates during these time periods exceeds the amount of displacement expected in a single earthquake from length-displacement scaling relationships (Wells & Coppersmith, 1994).

In their study, Mechernich et al. (2018) used two approaches to model the slip history of the Pisia fault, firstly adopting a manually iterative method based on the approach from Schlagenhauf et al. (2010) and secondly using the Bayesian MCMC modeling approach from Cowie et al. (2017). The Cowie et al. (2017) Flex code implements

Table 1
Inputs Used to Model Coseismic Vertical Deformation

Fault	Fault dips (deg)	Fault dip direction (deg)	Fault rake (deg)	Length of fault trace (km)	Mw	Slip at depth (m)	% Of slip at the surface
Pisia	60	355	−90	29	6.7	2.5	40
Skinos_Psatha	60	010	−90	22	6.4	0.9	40
Strava_Nixon	60	004	−90	22	6.63	2.7	40
Strava_Nixon	55	004	−90	22	6.63	2.6	40
Strava_Nixon	50	004	−90	22	6.63	2.5	40
Strava_Charalampakis	55	013	−90	10	6.18	1.2	40
Strava_Papatheodorou_Ferentinos	55	011	−90	10	6.18	1.2	40
Strava_Sakellariou	55	010	−90	8	6.05	1	40
Perachora_Nixon	60	352	−90	12	6.28	1.5	40
Perachora_Nixon	55	352	−90	12	6.28	1.4	40
Perachora_Nixon	50	352	−90	12	6.28	1.3	40

Note. 1981 Earthquake magnitudes and rupture traces are used to calculate deformation expected from the 1981 24 February Pisia and 25 February Skinos-Psatha earthquakes (Hubert et al., 1996; Jackson et al., 1982; Roberts, 1996a; Taymaz et al., 1991). Fault dip measurements for Pisia and Skinos-Psatha were obtained by measuring the dip of the fault free face and applied as representative values for the entire fault. See text (Section 5) for details of the modeling for the offshore Strava and Perachora faults which were modeled as part of the discussion (using fault traces from Charalampakis et al., 2014; Nixon et al., 2016; Papatheodorou & Ferentinos, 1993; Sakellariou et al., 2007). The Strava and Perachora fault earthquake magnitudes were calculated using fault length-displacement scaling relationships from Wells and Coppersmith (1994). For all faults modeled, the dip directions were obtained by drawing strike lines from the eastern to the western tips and adding 90° to this value. Slip at the surface was set at 0.4 (40%) of the slip value at depth, which is based upon the approach of Mildon et al. (2022) using data from Manighetti et al. (2007). Slip at depth is iterated in the code until it produces the observed (in the case of Pisia and Skinos-Psatha) or expected (in the case of Strava and Perachora) earthquake magnitudes.

the code of Schlagenhauf et al. (2010) within a Bayesian parameter estimation framework and attempts to find the best-fit slip history model that matches the ^{36}Cl concentrations. We opt to remodel the ^{36}Cl data set because the code from Beck et al. (2018), published since the Mechernich et al. (2018) paper, overcomes some of the modeling challenges that exist within the Schlagenhauf et al. (2010) and Cowie et al. (2017) approaches. Key differences between the Schlagenhauf et al. (2010) and Cowie et al. (2017) approaches compared to the Bayesian MCMC code from Beck et al. (2018) center around how the codes treat early ^{36}Cl production, the slip per earthquake, and the parameters involved in the production and preservation of ^{36}Cl (see Roberts et al. (2024) for a detailed explanation of the differences between the codes).

The Beck code requires input data files on (a) the rock and colluvial chemistry and densities, (b) paleomagnetic field and (c) geometry and locality measurements that relate to the fault scarp, its upper and lower slopes and the trench. These values are taken from Mechernich et al. (2018) and modeled using additional data on scaling for latitude and elevation (Table S1 in Supporting Information S1).

3.3. Models of Coseismic Vertical Deformation

To assess the role of fault-related uplift or subsidence on the present-day elevations of the Holocene coastal notches we model the expected vertical deformation caused by earthquakes based upon the 1981 Pisia and Skinos-Psatha earthquakes and using the fault traces of offshore faults. We model the expected uplift and subsidence using Coulomb 3.4 software (Toda et al., 2011) and the code of Mildon et al. (2016) (updated in Diercks et al., 2023), which allows the along-strike variability of the fault trace to be considered. Data inputs required to undertake this modeling are the fault trace, rake, dip and dip direction (Table 1). For the 1981 Pisia and Skinos-Psatha earthquakes, the lengths of the modeled fault traces were calculated from the magnitudes of the 24th and 25th February 1981 Pisia (Mw 6.7) and Skinos-Psatha (Mw 6.4) earthquakes (Jackson et al., 1982) using fault scaling relationships from Wells and Coppersmith (1994). The lengths of 29 and 22 km for the Pisia and Skinos-Psatha earthquakes, respectively, are similar to the lengths of the earthquake ruptures obtained from mapping after both earthquakes (Bornovas et al., 1984; Jackson et al., 1982; Mitchell et al., 2024; Roberts, 1996a). The slip distribution for each earthquake is automatically built by the code and assumes a simple bullseye/concentric slip distribution where maximum slip occurs in the center of the fault. For the Pisia and Skinos-Psatha earthquakes, values for subsurface slip were iterated until they produce the earthquake magnitudes observed. In the case of the deformation modeled on the offshore Strava and Perachora faults, the subsurface slip for each earthquake was chosen to match the earthquake magnitudes expected from using fault length-displacement scaling relationships (Wells & Coppersmith, 1994). The output fault slip distributions data are used to model the coseismic vertical deformation in Coulomb 3.4 (Toda et al., 2011), the results of which are displayed as 2D maps of vertical contours of uplift and subsidence expected at the surface. These maps were imported into Google Earth and the coseismic uplift or subsidence value for each contour is noted where it intersects with the north Perachora coastline. The modeled vertical motions were transposed onto graphs and presented along the strike of each fault trace.

4. Results

4.1. Compilation of Notch Elevations

We compiled notch mid-point, roof and floor elevations from along the north Perachora coastline using observations made during field campaigns in 2022–2023. Field observations were made at 10 locations over a 30 km transect between Sterna Bay (SteB) in the west and Psatha Bay (PsB) in the east (Figures 4 and 5; Table 2; for detailed locality information see Text S1 and Figure S1 in Supporting Information S1).

In the west of the research area, located in the hanging wall of the Pisia fault close to the tip, two subaerial notches are recorded at localities from Sterna Bay (SteB) to Scaliosa Beach (ScaB) along ∼6 km of coastline (Figures 4b–4g and 5b, Table 2). The highest observed notch has a mid-point elevation of 3.6 m at Scaliosa Beach (ScaB). Between Scaliosa Beach (ScaB) and Cave of the Seal (CoS) we observed a submerged notch(es) looking down from nearby sea-cliffs through clear water but were unable to snorkel at this location (at UTM (34S) 671361, 4216372, marked *X* on Figures 1 and 5a). Eastward from locality Cave of the Seal (CoS) the limestone coastline is located in the hanging wall of both the Pisia and Skinos faults with notches becoming submerged below sea level (Figure 5). Submerged notches were observed via snorkeling near Cave of the Seal (CoS), Strava Bay (StB) and Skinos Beach (SkB) (Figures 4h–4j). The deepest notch mid-point was measured at −1.65 m below sea level near Strava Bay. At Alkyonides Bay (AlB) and farther east at Psatha Bay (PsB) notches have been subaerially exposed in the footwall of the Skinos-Psatha fault as the fault transitions from onshore to offshore (Figures 4k and 5b, Table 2). Two kilometers directly north of the footwall notches at Psatha Bay we observe submerged notches in the hanging wall of the Skinos-Psatha fault.

We note that the wavelengths of the notches vary depending on whether they are subaerial or submerged (Figure 5b). Specifically, the wavelengths of subaerial notches between the floor and roof measurements measure between 0.9 and 3.4 m (average 1.73 m), compared to the submerged notches that have comparatively smaller wavelengths and measure between 0.25 and 0.8 m (average 0.6 m).

In summary, the observations on marine notches made herein show a transition from subaerial notches along the west of the north Perachora coastline, to submerged notches in the center of the coastline where subsidence from the Pisia and Skinos faults combine, and then back to subaerial notches along the east of the Perachora coastline as the Skinos fault moves offshore. The locations of observed subaerial and submerged notches agree with the locations of uplifting and subsiding coastline reported by Jackson et al. (1982). Furthermore, we show that throughout most of our localities on the north Perachora coastline, a sequence of only two notches are observed, whether notches are subaerial or submerged, compared to the four footwall notches reported at Heraion at the western tip of the Pisia fault investigated by Pirazzoli et al. (1994).

4.2. Slip History of the Pisia Fault From Re-Modeled ^{36}Cl Concentrations

Remodeling the ^{36}Cl concentrations measured from the Pisia fault scarp by Mechernich et al. (2018) (Figure 6a) was undertaken using the Bayesian MCMC approach of Beck et al. (2018) to recover fault slip histories. The slip history presented in Figure 6 (see Figure S2 in Supporting Information S1 for the full model results) shows results from a total of 836,920 model runs on two parallel Markov chains, comprising the least squares solution that provides the best fit to the data, an ensemble of the top 10,000 least squares solutions, and the 90% confidence bands according to the sampled posterior distribution and the ensemble of highest likelihood solutions after 50% burn-in from the posterior distribution (i.e., after 50% of the total model runs). The slip history that we interpret from these three visualizations (Figure 6b) implies that ^{36}Cl evidence for slip on the Pisia fault scarp is preserved since ∼40 ka according to the posterior distribution of highest likelihood solutions and the ensemble of the top

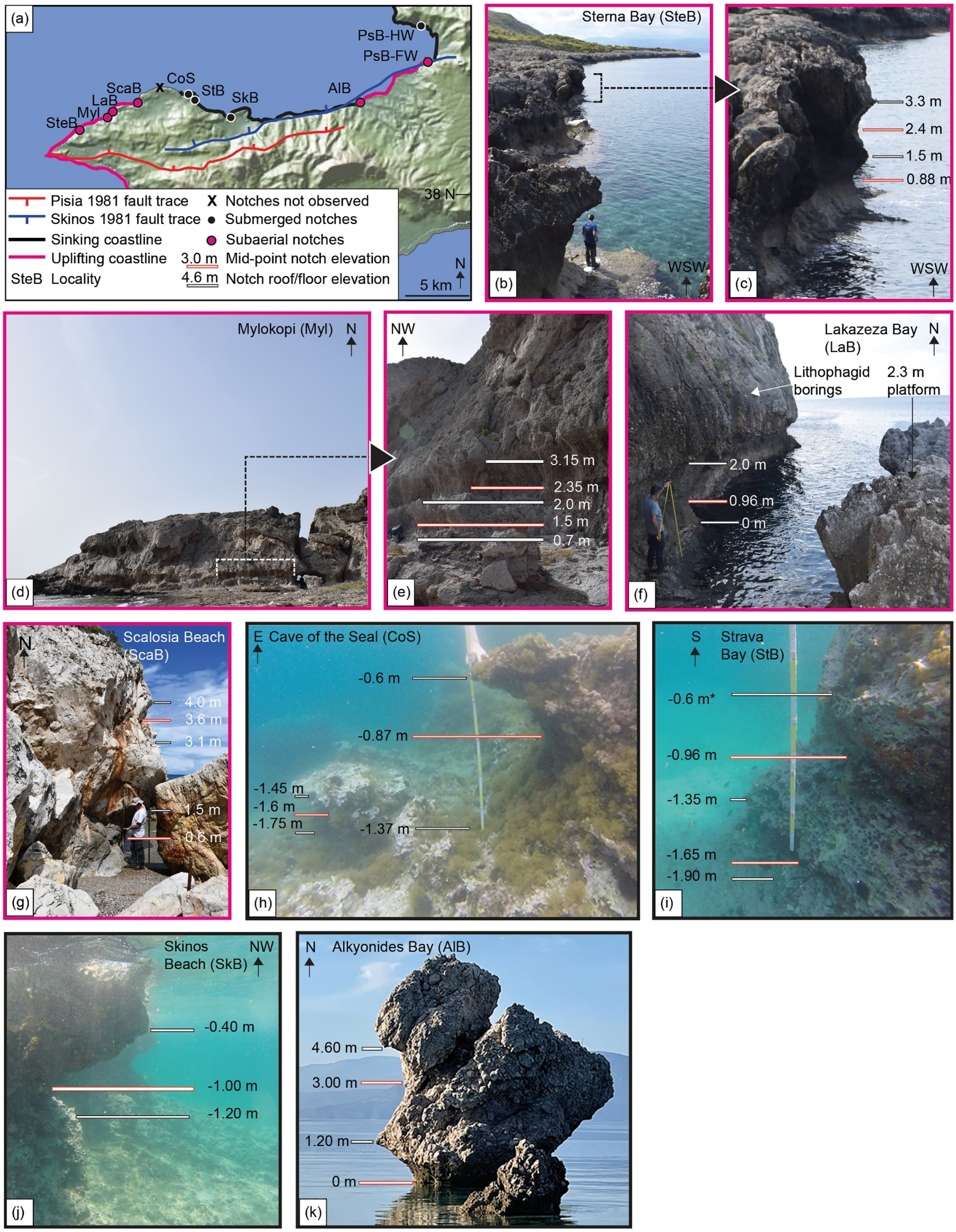

Figure 4. Marine notch localities (a) and photographs (b–k) show the measured mid-point, roof and floor elevations of the notches presented herein. Photos (h, i and j) were photographed beneath sea-level during snorkelling. Each white and yellow part of the ruler scale is 10 cm. NB. The lower notch at Cave of the Seal locality (h) is distorted by the perspective of the picture because it is further from the camera than the upper notch.

10,000 least squares solutions, with evidence for slip since ~30 ka suggested by the least squares solution (Figure 6b). Preservation of scarps evidencing surface faulting that occurred prior to the demise of the LGM have been observed elsewhere in Greece (e.g., Iezzi et al., 2021; Mechernich et al., 2023) and in the central and southern Apennines in Italy (Mildon et al., 2022; Roberts et al., 2024, 2025; Sgambato et al., 2025). Pre-LGM scarps are suggested to occur because the interplay between fault slip-rate and erosion rates allowed fault

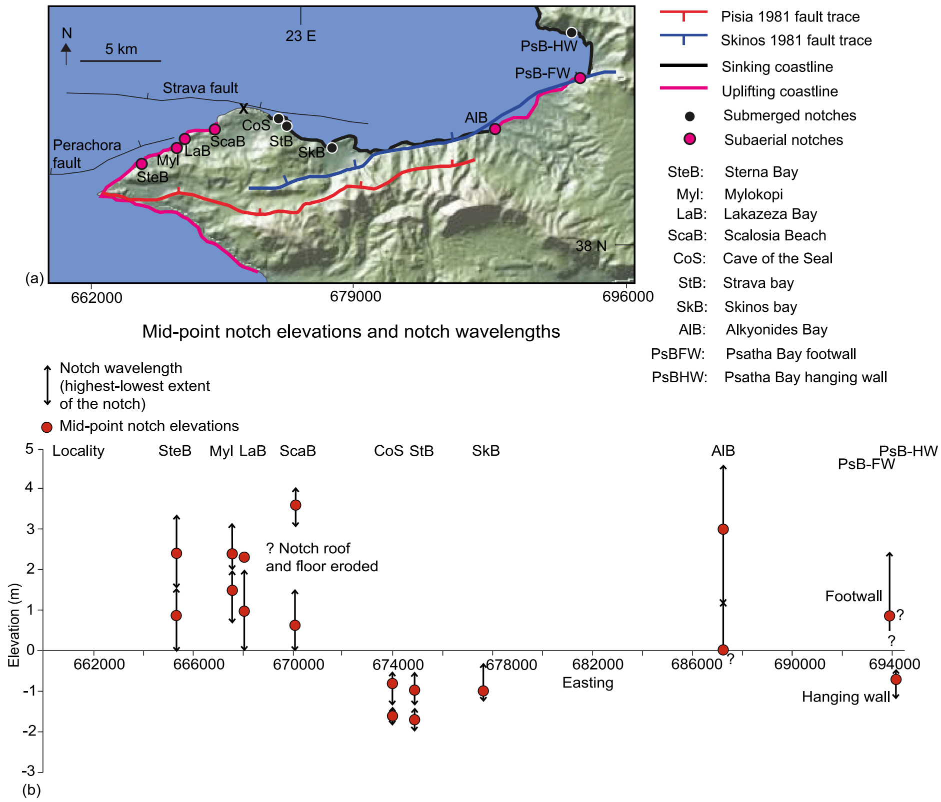

Figure 5. (a) Location of Holocene marine notch sites from which elevations were measured herein and their mid-point notch elevations (b). The vertical arrows in (b) represent the wavelength of the marine notch and are obtained from measuring the elevations of the roof and floor of the notches (Figure 2c).

scarp preservation, with older preservation promoted at lower elevations, presumably due to less frequent formation of ice promoting freeze-thaw action (Iezzi et al., 2021). The re-modeled slip history of the Pisia fault also shows temporal slip-rate fluctuations illustrated by the least squares solution and the changes in slope of the 90% confidence bands which bound the ensemble of least squares solutions (Figure 6b), this is further explored in a later section.

4.3. Coseismic Vertical Deformation Modeling

Elastic half-space deformation modeling of the expected vertical motions associated with the 24th and 25th February earthquakes on the Pisia and Skinos faults (see Section 3.4, Table 1 for the ruptured fault parameters) are used to examine whether combinations of such earthquakes can explain the spatial pattern of observed notch positions and elevations.

Modeled vertical deformation associated with the Pisia Mw 6.7 earthquake rupture trace predicts broad coseismic subsidence from the western tip of the Perachora Peninsula to close to Psatha Bay in the eastern extent of the research area (Figures 7b and 7c). Where we observe subaerial notches between localities Sterna Bay (SteB) and Scaliosia Beach (ScaB) coseismic subsidence associated with slip on the Pisia fault is relatively low, increasing from 0.2 m in the west (Sterna Bay) to 0.5 m in the east (at Scaliosia Beach). In the area between localities Scaliosia Beach (ScaB) and Cave of the Seal (CoS), where subaerial notches are not observed and where we have been unable to confirm the presence of submerged notches, modeled coseismic subsidence from the Pisia earthquake is ~0.45 m. In the area of observed submerged notches (Cave of the Seal (CoS) to Skinos Beach (SKB)), modeled Pisia earthquake coseismic subsidence is relatively large at 0.6–0.8 m (Figures 7b and 7c).

Modeling the deformation associated with the Mw 6.4 Skinos-Psatha earthquake shows less intense subsidence throughout the north Perachora coastline (Figures 7d and 7e). Where subaerial notches occur between Sterna Bay (SteB) and Scaliosia Beach (ScaB), the Skinos-Psatha coseismic subsidence reaches a maximum value of only

Table 2
Measurements of Notch Mid-Point, Roof and Floor Elevations

Site name	Easting	Center notch elevations (m)	Notch roof and floor values (m)	Notch wavelength (m)
Sterna Bay (SteB)	665323	0.88	**1.50**	1.5
			0.00	
		2.40	**3.30**	1.8
			1.50	
Mylokopi tombolo west/central (Myl)	667499	1.50	**2.00**	1.3
			0.70	
		2.35	**3.15**	1.2
			2.00	
Lakazeza beach west (LaB)	668047	0.96	**2.00**	2.0
			0.00	
		2.30	No observable notch	NA
Scaliosia beach (ScaB)	670038	0.60	**1.50**	1.5
			0.00	
		3.60	**4.00**	0.9
			3.10	
Cave of the seal (CoS)	674523	−0.87	**−0.60**	0.8
			−1.37	
		−1.60	**−1.45**	0.3
			−1.75	
Strava Bay (StB)	674844	−0.96	**−0.60**	0.8
			−1.35	
		−1.65	**−1.35**	0.6
			−1.90	
Skinos beach (SkB)	677762	−1.00	**−0.40**	0.8
			−1.20	
Alkyonides Bay (AlB)	687286	0.00	**1.20**	1.2
			0.00	
		3.00	**4.60**	3.4
			1.20	
Psatha Bay footwall (PsB-FW)	693935	0.90	**2.40**	2.4
			0.00	
Psatha Bay hangingwall (PsB-HW)	694183	−0.70	**−0.50**	0.7
			−1.20	

Note. All measurements were taken relative to sea level and have uncertainties of ±5 cm. The wavelength is the vertical distance between the measured roof and floor elevations. See also Figures 4 and 5. Notch measurements were taken 27 April 2022 (SteB), 18 September 2022 (ScaB), 22 September 2022 (LaB), 24–25 May 2023 (CoS, StB, SkB) and 15 September 2023 (Alb, PsB-FW/PsB-HW). Values in bold are notch roof measurements.

0.05 m. This value increases to between 0.1 and 0.2 m where we observe submerged notches (Cave of the Seal (CoS) to Skinos Beach (SkB)). Eastward, 2.5 km west of locality Alkyonides Bay (AlB), coseismic subsidence is modeled to a maximum of ∼0.3 m. Directly east of Alkyonides Bay (AlB) the Skinos-Psatha 1981 earthquake rupture is suggested to have stepped offshore onto the East Alkyonides fault and the coastline is modeled to experience very small coseismic uplift of <0.1 m.

When the modeled vertical deformation between the two 1981 earthquakes are compared, it is apparent that subsidence associated with the Pisia fault dominates the expected coastal motions in the area we have studied. For instance, at the location where submerged notches are observed (Cave of the Seal (CoS) to Skinos Beach (SkB))

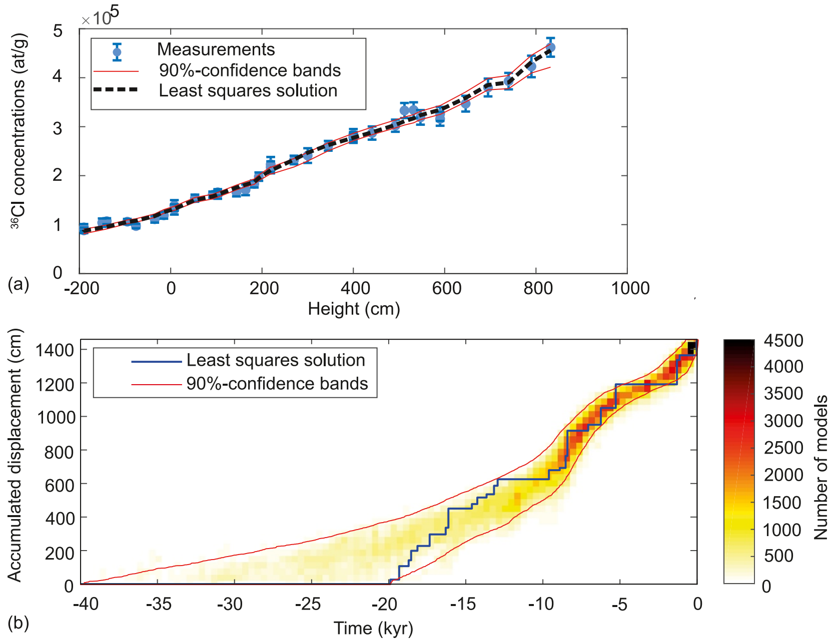

Figure 6. (a) ^{36}Cl concentrations reported in Mechernich et al. (2018) plotted against the height of the sample. (b) Slip history derived from modeling the ^{36}Cl concentrations using the Bayesian MCMC code (Beck et al., 2018). The least squares solution for the top 10,000 models is shown alongside the 90% confidence intervals from the posterior distribution. The Beck et al. (2018) code uses the overall shape of the height versus concentration graph in (a) for the samples removed from the preserved fault scarp to calculate likely slip scenarios for the eroded part of the fault scarp. This allows the best fit slip history beyond the extent of the preserved free face scarp to be inferred.

coseismic subsidence from the Mw 6.7 earthquake on the Pisia fault is four times greater than from the Mw 6.4 Skinos-Psatha earthquake (Figures 7c and 7e). Combining the modeled vertical deformation from both the 24 and 25 February earthquakes reveals the highest values of coseismic subsidence (0.6–0.95 m) where we observe submerged notches, specifically Cave of the Seal (CoS), Strava Bay (StB) and Skinos Beach (SkB) (Figure 7f). Our modeling also implies that the area directly east of Skinos Beach also experienced combined subsidence of up to 0.9 m. However, we have not explored whether submerged notches occur in this area because from the east of locality Skinos Beach (SkB) for ∼10 km the lithology is dominated by softer serpentinized ultrabasic rocks, which are significantly less affected by bioerosion and tends not to preserve coastal notches (Evelpidou et al., 2014). In the area directly west of locality Cave of the Seal (CoS) to Scaliosia Bay (ScaB) (Figure 1) where we could not access the sea, our modeling implies that this part of the coastline would have subsided by ∼0.5 m following the 24 and 25 February earthquakes (Figure 7e). Our observations from nearby sea-cliffs down through clear water is consistent with this.

5. Discussion

Overall, the results show that for the region near the Pisia fault: (a) Holocene coastal notch sequences occur at a variety of elevations relative to sea-level, and with a variety of numbers of notches and notch amplitudes, (b) the Pisia fault did not have a constant slip-rate, and (c) elastic half-space modeling reveals that coseismic slip on the Pisia fault would have dominated that of the Skinos-Psatha fault in deforming the coastline, with the area of maximum coseismic subsidence spatially coincident with the location of submerged notches.

5.1. Earthquake Clusters and Anti-Clusters and Their Relationship to Holocene Notch Formation

Interpreting the ^{36}Cl slip history of the Pisia fault (Figure 8) reveals high slip-rate episodes (accumulated displacement of ∼5.6 and ∼2.8 m), the amplitudes of which are too large to explain via single earthquakes of ∼1 m coseismic slip on the Pisia fault, defined by considering the expected coseismic slip given the fault length (Wells & Coppersmith, 1994; Wesnousky, 2008). Therefore, we interpret the high slip-rate episodes as temporal clusters of surface faulting earthquakes. Our interpretation of the timing of slip rate changes implies two

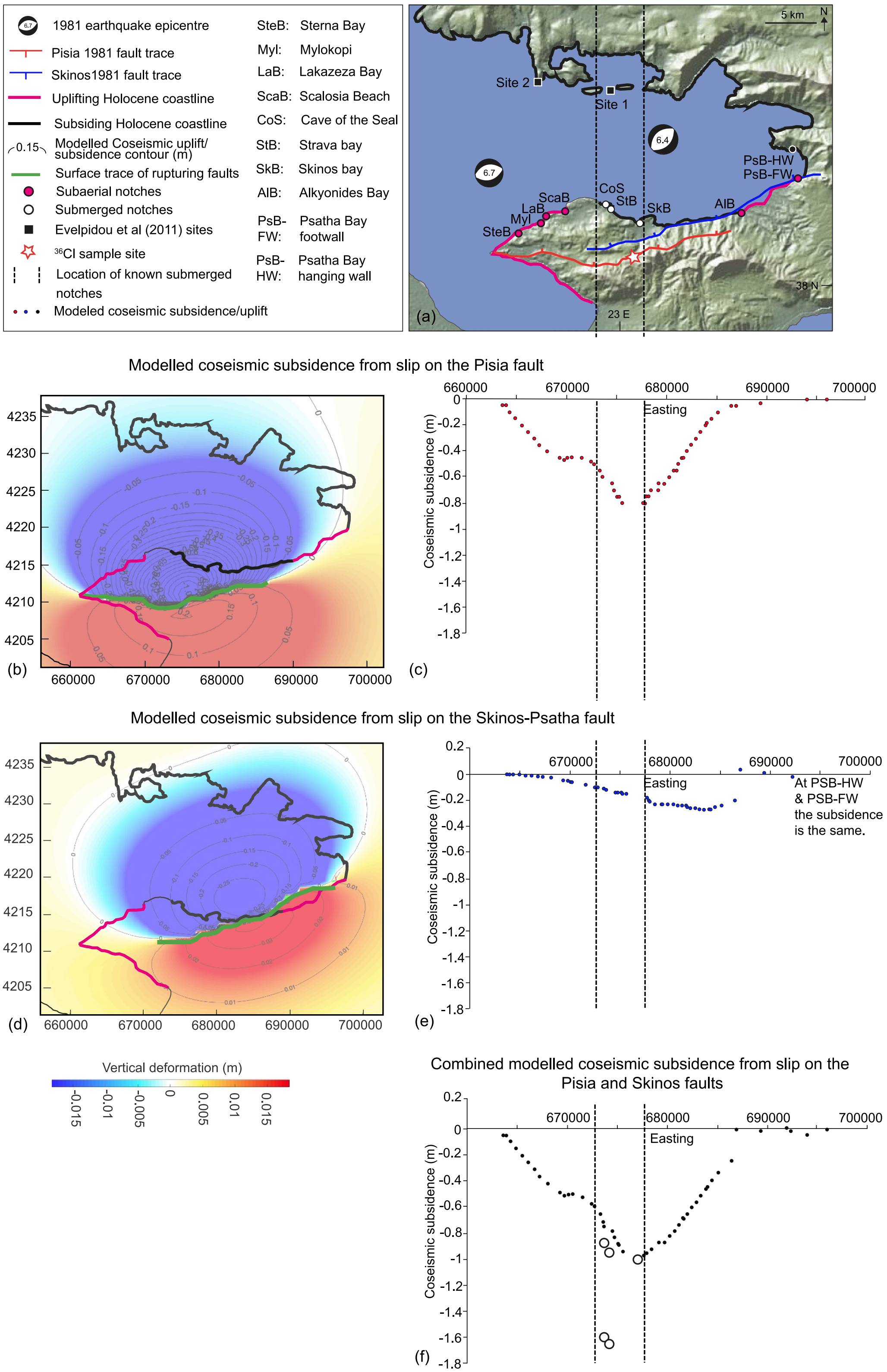

Figure 7. (a) Location of Holocene marine notch sites from which elevations were measured herein. Modeled coseismic deformation associated with the 1981 24 February Pisia (b, c) and 25 February Skinos-Psatha (d, e) earthquakes. (f) A plot of the summed coseismic modeled deformation from the Pisia and Skinos-Psatha earthquakes and measured submerged notch elevations (from Table 2). See Table 1 for input parameters into the model.

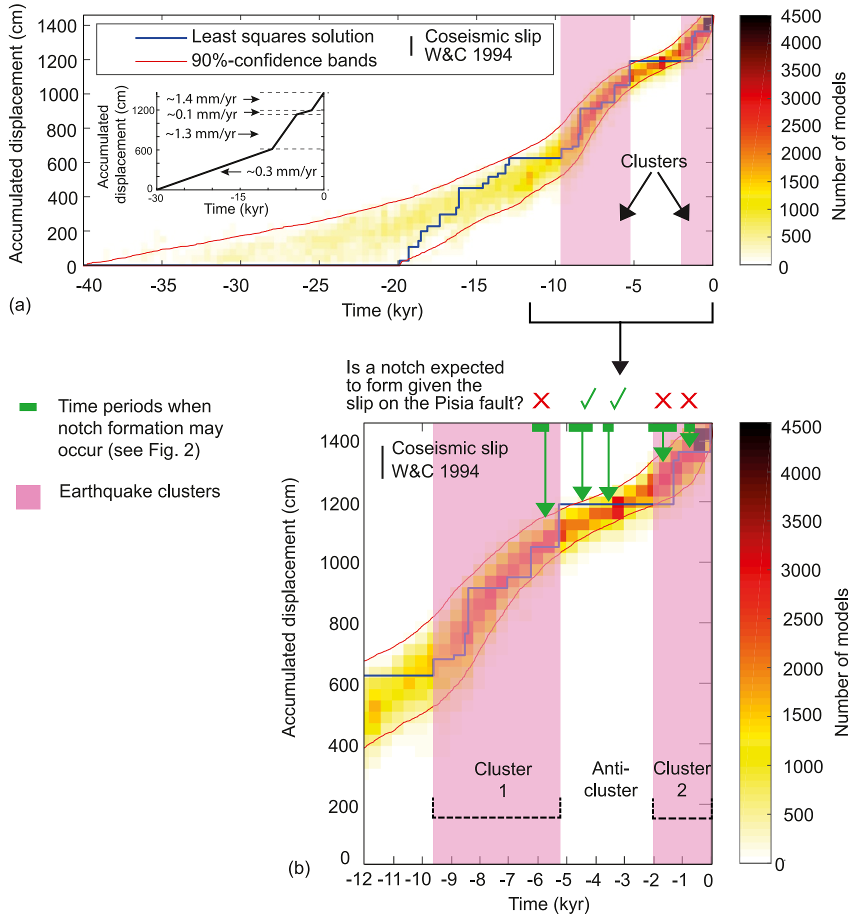

Figure 8. (a) Slip history derived from modeling the ^{36}Cl concentrations using the Bayesian MCMC code (Beck et al., 2018). The least squares solution for the top 10,000 models is shown alongside the 90% confidence intervals from the posterior distribution. The timing of earthquake clusters is inferred from the least squares solution, the density of least squares models and the changes in slip rate implied by the 90% confidence intervals. The expected coseismic slip is shown (derived from fault-length scaling relationships from Wells and Coppersmith (1994)) to demonstrate that the magnitude of slip recorded in clusters is greater than that expected from a single earthquake. Inset diagram provides an interpreted overview of the slip rates through time. (b) Presents the model from (a) since 12 ka overlaid with the timing of notch formation implied by the findings of Cooper et al. (2007) from Figure 2b. We use the timing of notch formation and the Pisia slip history to suggest that Holocene marine notches along the north Perachora coastline are not expected to have formed since 2.0 ka, but instead formed between 5.2 ± 0.5 and 2.0 ± 0.5 ka.

earthquake clusters from ~9.6 ± 0.5 to 5.2 ± 0.5 ka and ~2.0 ± 0.5 ka to 1981 (which we refer to herein as the “present day”) (Figure 8b). During cluster one (9.6 ± 0.5 to 5.2 ± 0.5 ka) the modeling implies that the fault accumulated 5.6 m of slip over ~4.4 kyrs (Figure 8b), resulting in a time averaged slip rate of 1.3 mm/yr. The fault appears to have entered an anti-cluster between ~5.2 ± 0.5 and 2.0 ± 0.5 ka, during which time little slip may have occurred. The 3.2-kyrs duration of this period of relative quiescence is comparable to those observed on other fault scarps that have been dated with ^{36}Cl (Iezzi et al., 2021; Mechernich et al., 2023; Mildon et al., 2022; Roberts et al., 2024, 2025). Cluster two is observed from 2.0 ± 0.5 ka to the present day, during which time interpretation of the results is that 2.8 m of slip has occurred (1.4 mm/yr slip rate). Earthquake slip during cluster two includes 1.1 m measured at the ^{36}Cl site associated with the 24 February 1981 Mw 6.7 Pisia earthquake (our measurements and from Mechernich et al. (2018); Mitchell et al. (2024)). We note that the timing of clusters identified using the ^{36}Cl slip history remains consistent when the dimensions of the pixels within the ensemble of least squares solutions are adjusted (Figure S3 in Supporting Information S1). In the Beck et al. (2018) code, the dimensions of the pixels are defined by the user. Adjustments made to the dimensions of the pixels within the ensemble of least squares solutions changes the visualization of the model results and the number of models represented by each pixel. Our analyses indicate that the timing of earthquake clusters and anti-clusters identified herein are not sensitive to the selected pixel sizes we have modeled.

To summarize, two distinct earthquake clusters are interpreted from the slip history, the first between ∼9.6 ± 0.5 to 5.2 ± 0.5 ka with a time averaged slip rate of 1.3 mm/yr and the second from 2.0 ka to the present day with a time averaged slip rate of 1.4 mm/yr. We suggest that the slip histories presented herein and from Mechernich et al. (2018) show broad agreement, specifically when the two outputs of the MCMC modeling approaches in each study are compared. These similarities are also apparent in Iezzi et al. (2021, see their Text S3b in Supporting Information S1) who undertook a brief comparison of the Pisia slip histories that Mechernich et al. (2018) derived using the Cowie et al. (2017) Flex code and that which Iezzi et al. (2021) produced using the Beck et al. (2018) code.

We compare our ^{36}Cl slip history with the possible timing of notch formation and emergence along the Perachora coastline. Notch formation requires a stable sea level and coastline that is not actively subsiding (e.g., Cooper et al., 2007; Evelpidou et al., 2014; Trenhaile, 2015). The ^{36}Cl slip history implies that from 5.2 ± 0.5 ka to 2.0 ± 0.5 ka the Pisia fault was in an anti-cluster (as defined by Roberts et al., 2024, 2025) because it experienced very little, if any slip, implying a slip rate lower than the long-term slip rate from ^{36}Cl data over the last ∼30 kyrs (Figure 8). We hypothesize that the notches must have formed in this ∼3.2-ka period when the Pisia fault was not actively subsiding the coastline. It is reassuring that our hypothesis fits with the ∼5 ka radiocarbon age associated with the highest and oldest dated notch on the north coast at Locality Mylokopi (Sample 92PE8 from Pirazzoli et al., 1994). Whilst this 3.2-kyr period also coincides with two potential notch forming events (Figure 8b) identified by Cooper et al. (2007), we note that our model allows for notches to form at any time throughout the period of Pisia's anticluster. Notch formation from 2.0 ± 0.5 ka to the present day was not possible given that the Pisia fault was in an earthquake cluster over this period (Figure 8) and actively down-throwing the coastline. In other words, the coastline was not in a stable position during the recent cluster to allow the formation of notches. Furthermore, the same is true of the time period between ∼9.6 ± 0.5 ka and ∼5.2 ± 0.5 ka when sea-level was rising after the demise of the last glacial maximum, so notches could not form due to the high slip-rate and unstable sea-level.

In summary, the slip history we derive for the Pisia-Skinos fault from remodeling ^{36}Cl concentrations from Mechernich et al. (2018) implies two periods of high slip occur from ∼9.6 ± 0.5 to 5.2 ± 0.5 ka and 2.0 ± 0.5 ka to the present day. We interpret these high slip periods as earthquake clusters. Furthermore, and of importance for this paper, we note that between ∼5.2 ± 0.5 ka to 2.0 ± 0.5 ka relatively little fault slip occurred, implying an anti-cluster lacking significant surface faulting, so that the Pisia fault would not have been deforming neighboring coastlines at this time.

5.2. Modeled Coseismic Deformation Within the Context of Measured Notch Elevations

Our modeled coseismic vertical motions (Figure 7) agree with observations of coastal deformation associated with the 1981 earthquake sequence. This is clear when we compare our locations of modeled coseismic uplift and subsidence with those observed from post-earthquake mapping (Hubert et al., 1996; Vita-Finzi & King, 1985) and through comparison of pre- and post-seismic triangulation data collected by the Hellenic Military Geographic service (reported in Stiros and Pirazzoli (1998)). This latter data set reported subsidence of up to 0.85 m in the hanging wall of the ruptured faults, a value similar to that obtained herein in our coseismic vertical deformation modeling (Figure 7e). Furthermore, we observe that the subsidence modeled on the coastline that bounds the north of the Alkyionides Gulf agrees with the locations of submerged notches observed along this coastline by Evelpidou et al. (2011) (Figure 1). Taken together, we use this evidence to suggest that our coseismic vertical deformation of coastal deformation along the northern Perachora coastline is consistent with the motion that occurred during 1981 24 and 25 February Pisia and Skinos-Psatha earthquakes.

Given the recent Pisia and Skinos-Psatha earthquakes in 1981, it is necessary to consider the effects of post-seismic slip/relaxation in the context of our modeling. Mildon et al. (2024) investigated transient slip on the Pisia and Skinos faults since 2016. In doing so Mildon et al. (2024) re-measured piercing point surface ruptures associated with the 1981 earthquakes to investigate post-seismic after-slip and noted that their measurements in 2023 have not changed since the initial measurements made in 2001. Mildon et al. (2024) also show that post-seismic visco-elastic relaxation associated with the 1981 earthquakes is likely to be minimal and in the order of 0.5 mm/yr which equates to 21.5 mm since the 1981 earthquakes. Whilst we cannot constrain any post-seismic after-slip/relaxation on the Pisia and Skinos faults as a result of earthquakes prior to 1981, the results from Mildon et al. (2024) provide some insight into the magnitude of post-seismic relaxation in the hanging wall and footwall of the Pisia and Skinos faults.

Comparison of the combined pattern of modeled coseismic deformation (Figure 7f) with our observations of subaerial and submerged notches (Figure 5b) shows that the areas of greatest modeled subsidence coincide with the locations of submerged notches at localities Cave of the Sea (CoS), Strava Bay (StB) and Skinos Beach (SkB) (Section 4.3). The measured notch mid-point elevations at these localities reveals that the elevations of the deepest submerged notches (1.6 m at Cave of the Seal (CoS) and 1.65 m at Strava Bay (StB) (Figure 5)) are more than the 0.95 m maximum subsidence modeled from the 1981 Pisia and Skinos-Psatha earthquakes (Figure 7e), suggesting that more than one earthquake on the Pisia (and Skinos?) faults have occurred since the formation of the notches.

5.3. Present-Day Notch Elevations Linked With the Pisia Fault ^{36}Cl Slip History

Our interpretations suggest that the timing of the Pisia fault anti-cluster would have allowed formation of notches between 5.2 ± 0.5 ka and 2.0 ± 0.5 ka, with notches not able to form at other times due to relatively high slip-rates and/or rates of early Holocene sea-level rise (Section 5.1). We also show that the magnitude of modeled coseismic subsidence is not great enough to produce the observed magnitudes of coastal deformation, so more than one earthquake sequence like that in 1981 is required (Section 5.2). However, we have not yet used our findings to determine: (a) the link between the finite geometry of the deformed notch sequence along strike and the earthquake clustering in the late Holocene implied by the ^{36}Cl results, or (b) the influence of other faults in the region such as those offshore within the Gulf of Alkyonides. Addressing these points is the focus of the following section.

To investigate whether the present-day notch observations can be explained by faulting implied by the ^{36}Cl slip history we restore the elevations of the notches back through time using the slip on the Pisia fault in its most recent cluster (2.0 ± 0.5 ka to the present day). We do this using our measurements of the notch mid-point elevations (Figure 5) and the modeled uplift/subsidence obtained from our elastic half-space vertical deformation modeling (Figure 7). The Pisia ^{36}Cl slip history implies 2.8 m of slip in cluster two since 2.0 ± 0.5 ka (Figure 8), and we know that during the 1981 Mw 6.7 Pisia earthquake the coseismic slip at the site of ^{36}Cl sampling was 1.1 m (Mechernich et al., 2018). Assuming that previous earthquakes on the Pisia fault have similar slip distributions, the equivalent of 2.8 1-m slip events need to have occurred between 2.0 ± 0.5 ka and the present day to explain the slip derived from modeling the ^{36}Cl concentrations. We use the fact that the Pisia and Skinos faults slipped broadly coevally in 1981, that is within a few hours, to imply that much like the 1981 event when the Pisia fault slips in the past, the Skinos fault may also slip. With this in mind, we restore the present-day notch elevations to their expected elevations prior to the vertical deformation associated with 2.8 earthquakes on the Pisia and Skinos-Psatha faults. We do this using the uplift/subsidence values modeled from the 1981 Pisia and Skinos-Psatha earthquakes (Figure 7) to adjust the present-day notch elevations (Figure 5) to the elevations expected prior to cluster two beginning at 2.0 ± 0.5 ka. We model the simplest scenario of two 1981-type earthquakes and a smaller earthquake that causes 80% of the uplift/subsidence associated with a 1981-type earthquake. For instance, at locality Strava Bay (StB) the observed mid-point elevations of the submerged notches are −0.96 and −1.65 m below sea level (Figure 5) and the combined modeled coseismic subsidence from the Pisia and Skinos-Psatha earthquakes is 0.85 m (Figure 7e). Thus, in 2.8 earthquakes this part of the coastline is expected to have been downthrown by ∼2.38 m. Figure 9 shows that removing the effect of this subsidence from the measured mid-point notch elevations at Strava Bay restores the notches to 1.4 and 0.7 m above sea level. Restoring all mid-point notch elevations (Figure 9) using the modeled coseismic uplift/subsidence reveals that the present-day subaerial notches would have slightly higher expected elevations and the submerged notches at Cave of the Seal (CoS), Strava Bay (StB) and Skinos Beach (SkB) would be relocated subaerially. We recognize that this is a simplified approach because we cannot determine the slip distribution of earthquakes prior to the 1981 event. Also, if our assumption that Pisia and Skinos always slip coevally is incorrect, then we do not expect the elevations presented in Figure 9b to change too significantly because slip on the Pisia fault causes ∼80% of the total subsidence in the location of submerged notches (Figure 7).

In our model of the pre-2.0 ± 0.5 ka restored notch elevations (Figure 9) subaerial notches occur throughout the length of the north Perachora coastline (with the exception of the Psatha Bay hanging wall, PsB-HW). The source of uplift of the subaerial notches needs to be considered. The offshore Strava fault (Figure 1) has been cited in other studies as being the possible cause of Holocene notches along the north Perachora coastline (e.g.,

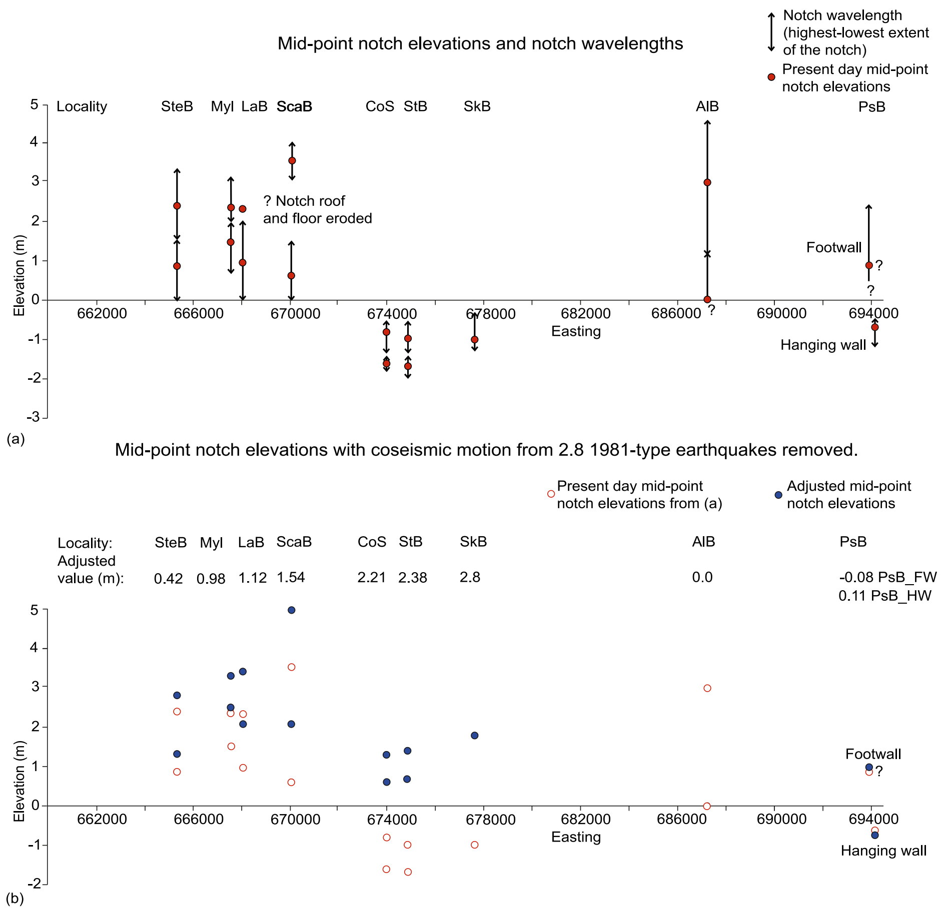

Figure 9. (a) Measured mid-point notch elevations reported in this study. (b) Elevations of the mid-point notch elevations (blue) that are hypothesized prior to the 2.0 ± 0.5 ka Pisia earthquake cluster (see text for an explanation of the method adopted to restore the notches to their pre-2.0 ± 0.5 ka elevations).

Schneiderwind, Boulton, Papanikolaou, & Reicherter, 2017). Whilst the proximity of the center of the Strava fault to the uplifted notches on the northern Perachora coastline makes it a likely candidate to cause coastal uplift, the role of the offshore Perachora fault (Figure 1) also needs to be considered. We conducted coseismic vertical deformation modeling using the same approach in Section 3.3 to explore whether the restored notch elevations at ∼2.0 ka (Figure 9) can be explained by slip on the Strava or Perachora faults. This test compares the modeled spatial patterns of coseismic uplift from the Strava and Perachora faults to the spatial pattern of restored upper notch mid-point elevations from along the north Perachora coastline. Herein we use the Strava and Perachora fault traces implied by the offshore fault map from Nixon et al. (2016) (Figure 1) because this fault map is compiled by integrating all offshore Corinth Rift seismic data. Owing to uncertainty regarding the dips of the Strava and Perachora faults (e.g., Sakellariou et al., 2007), we also model vertical deformation using fault dip values of 50°, 55° and 60° (Table 1). Furthermore, we test the sensitivity of our uplift modeling using different Strava fault traces from the literature (Charalampakis et al., 2014; Papatheodorou & Ferentinos, 1993; Sakellariou et al., 2007). For each fault we use the length of the fault trace to calculate the expected earthquake magnitude (using fault-length scaling relationships from Wells and Coppersmith (1994)) (Table 1). The 12 km fault length of the Perachora fault from Nixon et al. (2016) is calculated to produce a Mw 6.28 earthquake, whilst the 22 km Strava fault from Nixon et al. (2016) would produce a Mw 6.63 earthquake (Table 1). We note that the modeled magnitude of the Strava fault is similar to that suggested by Schneiderwind, Boulton, Papanikolaou, and Reicherter (2017) (Mw 6.7) to have caused the Mylokopi notch sequence.

Our vertical deformation modeling (Table 1) of the Strava fault trace (Nixon et al., 2016) with a dip of 60° reveals maximum coseismic uplift is modeled between localities Lakazeza Beach (LaB) and Scaliosa Beach (ScaB) (Figures 10b and 10c). The coseismic footwall displacement gradient modeled from slip on the Strava fault appears

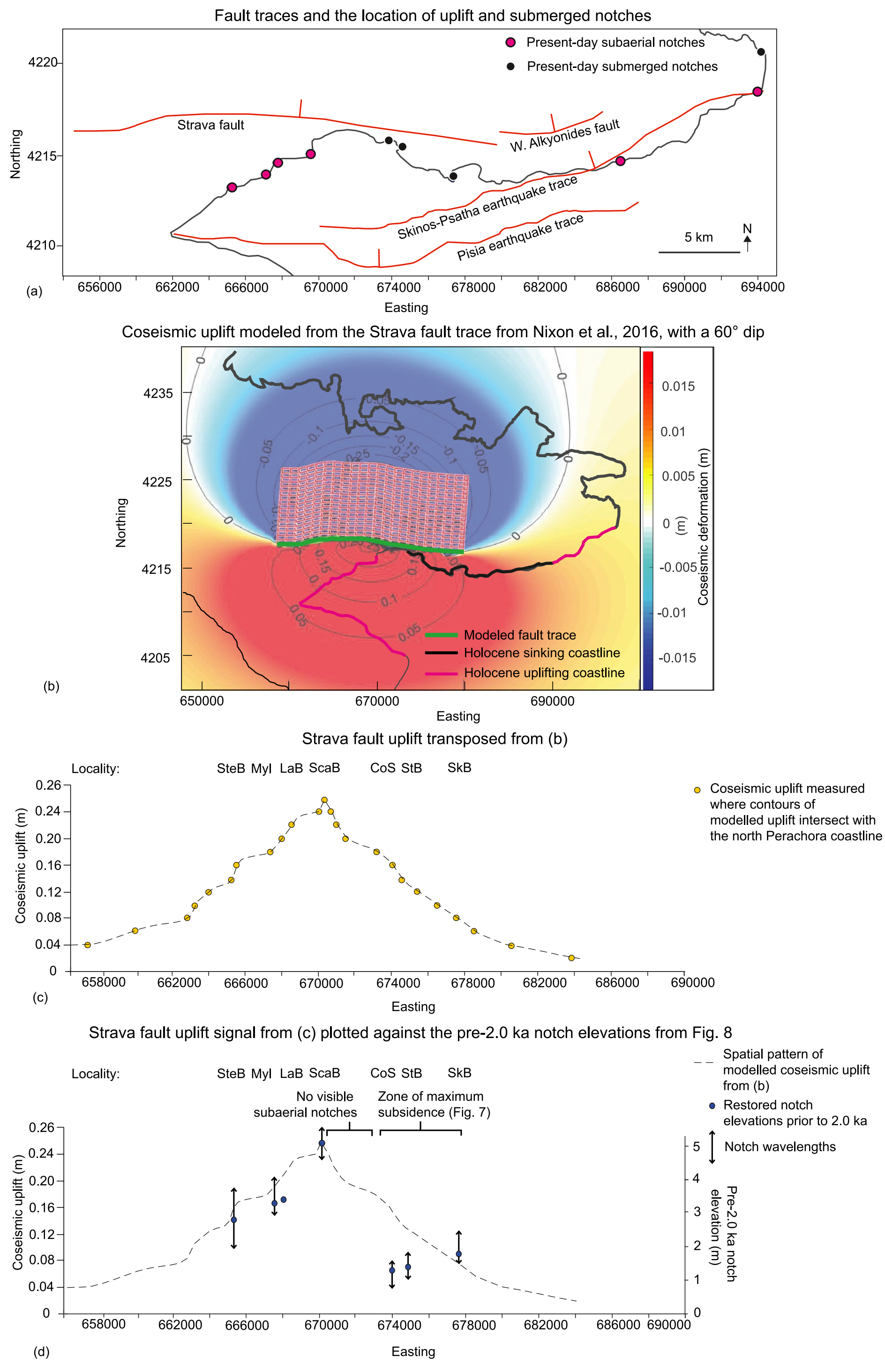

Figure 10. (a) Simplified fault map, the offshore fault traces are from Nixon et al. (2016). (b) Coseismic uplift modeled using vertical deformation modeling in an elastic half space (Section 3.3) for the Nixon et al. (2016) 22 km long Strava fault trace with a 60° dip (see Figure S4 in Supporting Information S1, for the coseismic uplift results for modeling (i) the Strava fault trace from Nixon et al. (2016) with dips 55° and 50°, (ii) other Strava fault traces from the literature and (iii) the Perachora fault trace from Nixon et al. (2016)). (c) Plot of the coseismic uplift modeled using vertical deformation from (b). (d) Spatial pattern of coseismic uplift modeled on the Strava fault from (c) overlaid with the restored notch elevations from Figure 9.

to broadly agree with the spatial pattern of the upper restored notches at ~2.0 ka, at least in the west of the profile (Figure 10d). We see this pattern of uplift regardless of the dip used to model slip on the Strava fault, noting that the magnitude of uplift changes slightly with changing dip values (Figures S4a–S4d in Supporting Information S1). Furthermore, we note that modeled uplift from slip on alternative Strava fault traces (Table 1) yields similar spatial patterns of footwall uplift to those modeled using the fault trace from Nixon et al. (2016) (Figures S4e–S4j in Supporting Information S1), again with variation observed in the magnitude of uplift. The spatial uplift pattern implied by slip on a 60°-, 55°- and 50°-dipping Perachora fault varies significantly to that observed on the upper restored notches. Specifically, the upper restored notches increase in elevation from west to east but slip on the Perachora fault is modeled to cause decreasing uplift from west to east (Figures S4k–S4p in Supporting Information S1). Consequently, we discount the Perachora fault as being the dominant cause of the uplifted Holocene notches.

We interpret the results of our vertical deformation modeling to imply that it is plausible that the uplifted notches on the north Perachora coastline were produced by slip on the offshore Strava fault, in particular noting good agreement between the spatial footwall displacement profile from rupturing the Strava fault according to the Nixon et al. (2016) fault trace. Whilst the restored elevations in the west of the study area agree well with the spatial pattern of coseismic uplift (Figure 10d), the fit between the restored notches closer to the middle of the fault system at Cave of the Seal (CoS), Strava Bay (Stb) and Skinos Beach (Skb) and the spatial pattern of coseismic footwall uplift is poor (Figure 10d). We suggest that because these notches (at CoS, StB and SkB) also occur in the hanging wall of the Skinos fault, the lack of fit may be explained by slip on the Skinos fault that could have occurred during the Pisia fault anti-cluster that our model has not taken into account and would act to slightly reduce the overall uplift caused by slip on the Strava fault.

Based on our assumption that the observed upper notch along the coastline is associated with formation at ~5 ka (Section 4.2, Figure 8b), the Strava fault is expected to have been slipping since ~5.2 ± 0.5 ka (when the Pisia fault was in an anti-cluster) throughout the time taken for two notches to form. We suggest that the fact that the wavelengths of subaerial notches are larger compared to submerged notches (Figure 5b) supports our assertion that footwall uplift has driven deformation of the present-day subaerial notches. Elongated notch wavelengths are expected to occur because individual earthquakes would uplift a notch originally at or close to sea level by up to few decimeters per event (e.g., Schneiderwind, Boulton, Papanikolaou, & Reicherter, 2017). Such coseismic values are not high enough to fully remove the notch out of the ~20 cm tidal range within the Mediterranean (Evelpidou, Kampolis, et al., 2012; Tsimplis, 1994), instead producing notches with enhanced amplitudes.

Drawing together our ^{36}Cl slip history and the restored and present-day notch elevations allows us to hypothesize the order of events, which we explore using the notch elevation measurements at locality Strava Bay (StB). Firstly, cluster 1 on the Pisia fault ends at 5.2 ± 0.5 ka, we do not expect a Holocene notch to have formed by 5.2 ± 0.5 ka because the coastline was not tectonically stable and the sea level did not stabilize until 7.0–6.5 ka (Figure 11a). The Pisia fault then enters into an anti-cluster. Two notches form between 5.2 ± 0.5 ka and 2.0 ± 0.5 ka as a result of footwall uplift that we associate with an earthquake cluster on the Strava fault (Figure 11b). From this point onward there are two potential explanations for the present-day notch locations. The first explanation (Figure 11c) is that coastline uplift continues after the formation of the second notch as a result of continued slip on the Strava fault, raising the lowest notch to 0.73 m above sea level (as per the adjustment made in Figure 9 for Strava Bay (StB) removing the effect of 2.8 earthquakes on the Pisia and Skinos faults (2.38 m) from the measured lowest notch elevation of −1.65) (Figure 11d). At 2.0 ± 0.5 ka the Pisia fault then enters into an earthquake cluster causing the notches to move to their present-day elevations (Figure 11f). Specifically, the subaerial notches located close to the center of the fault system become submerged. An alternative explanation (Figure S5 in Supporting Information S1), is that the lowest notch remains at sea level following its formation until the Pisia fault then becomes active at 2 ka (Figure S5d in Supporting Information S1). In this scenario, the Pisia fault would downthrow the coastline through its sequence of earthquakes whilst the Strava fault continues to be active and produce comparatively small coseismic uplift events (Figures S5e and S5f in Supporting Information S1). The comparatively small coseismic uplift associated with an earthquake on the Strava fault (0.1 m at locality Strava Bay, Figure 10) would be dominated by coseismic subsidence from the Pisia fault (0.8 m, Figure 7), with slip on both faults contributing to placing the notches in their present day position. The key difference between these two explanations is that in the first (Figure 11), the Strava fault is not active at the same time as the Pisia fault, while in the alternative scenario both the Pisia and Strava faults are active from 2 ka to the present day (Figure S5 in Supporting Information S1). Whilst our data alone do not allow us to differentiate

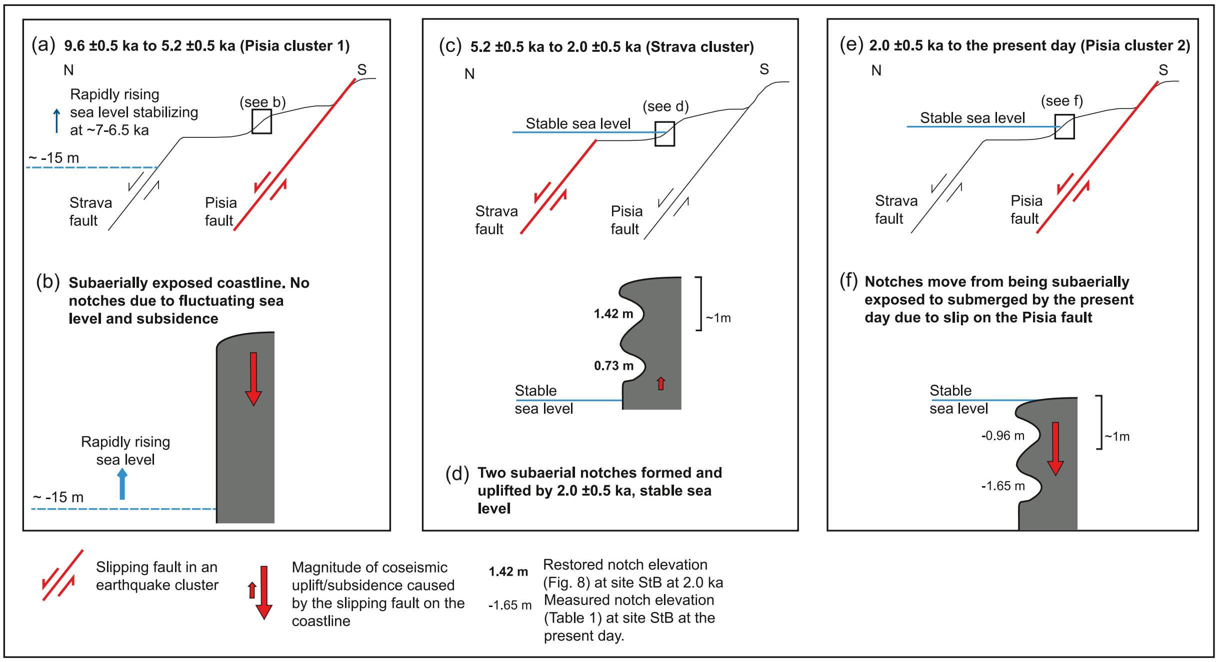

Figure 11. Hypothesized order of events to explain the present-day notch elevations (illustrated using the example of Strava Bay (StB), see Table 1 and Figure 9). (a) 9.6 ± 0.5 ka to 5.2 ± 0.5 ka, the Pisia fault is slipping in a cluster (Figure 8) down-throwing the coastline, sea-level is rapidly rising and not stable (Figure 2). (b) At the end of the Pisia cluster in (a) no notches are expected to form because the coastline is not tectonically stable and sea-level has not stabilized following demise of the LGM. (c) 5.2 ± 0.5 ka to 2.0 ± 0.5 ka the Pisia fault is in an anti-cluster (Figure 8), and we suggest the Strava fault was slipping. (d) At the end of the Pisia anti-cluster at 2.0 ± 0.5 ka two notches have formed and experienced footwall uplift caused by slip on the Strava fault. Note that the magnitude of Strava fault coseismic footwall uplift is not expected to exceed ~0.15 m at StB (Figure 10). Notches can form during this period because the coseismic uplift values from slip on the Strava fault are smaller than the tidal range within the Gulf. (e) 2.0 ± 0.5 ka to the present day, the Pisia fault enters a cluster (Figure 8). (f) During the time period in (e), slip on the Pisia fault subsides the coastline and two notches are submerged below sea level to their present-day elevations.

between which scenario is true, the findings of recent studies can provide some insight. Normal faults have been shown to display episodic temporal earthquake behavior with ^{36}Cl slip histories revealling that temporally coeval earthquake clusters rarely occur on faults located across strike to one another (where distance between such faults is 5–15 km) (Iezzi et al., 2021; Mildon et al., 2022; Roberts et al., 2024, 2025; Sgambato et al., 2025). In these instances, one fault within the parallel fault system is actively accommodating the tectonic extension whilst other across strike faults are quiescent and exhibit anti-clusters. Given the spacing between the Strava and Pisia faults (~7 km), we suggest it is plausible that slip on the Pisia fault would inhibit coeval slip on the Strava fault. Therefore, we favor the first explanation (Figure 11) as the possible order of events.

Our preferred order of events detailed in Figure 11 implies that the Strava fault was active and uplifting the coastline during the period of quiescence on the Pisia fault between Cluster one and Cluster two (Figure 8). If our favored hypothesis of the sequence of events above is correct, we can explore the timing of slip on the offshore Strava fault throughout the late Holocene. Whilst previous studies recognize that the Strava fault has been active throughout the Holocene, deformation rates associated with the fault are lacking (Bell et al., 2009; Leeder et al., 2005; Sakellariou et al., 2007). However, it is clear from the reported presence of Pleistocene paleoshoreline sequences in the western 7 km of the northern Perachora coastline (Collier et al., 1992; Dia et al., 1997; Evelpidou et al., 2023; Kershaw & Guo, 2003; Leeder et al., 2003, 2005; Morewood & Roberts, 1997, 1999; Robertson et al., 2020) that the long-term signal appears to be uplift. Using the data presented herein and from estimates of the uplift to subsidence ratio on a fault, we can approximate the slip rate on the Strava fault. We calculate the Strava fault slip rate over the recent Holocene using uplift to subsidence ratios of 1:2 and 1:3 (e.g., de Gelder et al., 2019; McNeill et al., 2005; Papanikolaou et al., 2010) and the restored elevation (3.4 m) of the upper notch at Lakazeza Beach (LaB, Figure 9b). The restored elevations are used in these calculations because we do not want to include any contribution from slip on the Pisia and Skinos-Psatha faults. We calculate the timing of possible slip on the Strava fault as occurring from when the first notch formed (~5.2 ka) up to 2.0 ka, but we accept that clustered slip may have occurred over a time period shorter than 3.2 ka in which case the slip rates would be higher. Uplift to subsidence ratios of 1:2 and 1:3 imply the Strava fault slip rates may be in the range of 3.7–4.9 mm/yr during the 3.2-kyrs period of its hypothesized cluster (calculated using an uplift rate of 1.1 mm/yr from the elevation of the assumed ∼5.2 ka notch mid-point and assuming that the Strava fault dips at 60°). A slip rate of 3.7–4.9 mm/yr is plausible in a cluster as values of this magnitude have been reported from other slip histories implied by ^{36}Cl on normal faults (e.g., Iezzi et al., 2021; Mechernich et al., 2023; Mildon et al., 2022; Roberts et al., 2024, 2025) and considering that geodetic extension rates across the eastern Gulf of Corinth are ∼5 mm/yr (Briole et al., 2000, 2021; Clarke et al., 1998; Davies et al., 1997). Our study highlights that the interplay between the fault displacement gradients and the timing of earthquake clusters from faults across strike has the capacity to result in complex along-strike patterns of uplift and subsidence which is pertinent to studies that use deformed coastlines to investigate faulting. We also suggest that the results of our study may be used to contribute toward improved understanding of the mid to recent Holocene sea levels in the Gulf of Corinth and wider Mediterranean. Tectonically active locations are rarely used to investigate past sea levels because the tectonic motion of the coastline contributes significantly to uncertainty associated with past sea level (Lambeck et al., 2004). However, we suggest that the timings and magnitudes of slip provided by ^{36}Cl data, such as those presented herein, may contribute to understanding the tectonic component.

Accepting our preferred timing of events (Figure 11) implies that the across strike Pisia and Strava faults may slip out of phase with one another. Out of phase slip is a common theme emerging from fault studies throughout the world, where slip rates evaluated over timescales of tens of thousands of years and more reveal that earthquake clusters on across strike normal and strike-slip faults rarely occur at the same time, with the actively slipping fault accommodating high proportions of the regional strain (Bennett et al., 2004; Dolan et al., 2024; Friedrich et al., 2003; Gauriau & Dolan, 2024; Iezzi et al., 2021; Meschis et al., 2022; Mildon et al., 2022; Roberts et al., 2024, 2025). Such studies provide evidence that crustal-scale fault activity may alternate between closely spaced faults across strike with one fault experiencing high slip rates within a cluster relative to its long-term averaged slip rate. Consequently, geodetic observations over shorter decadal timescales may not always reliably identify potentially seismically hazardous faults (e.g., Gauriau & Dolan, 2024; Iezzi et al., 2021; Roberts et al., 2024). We suggest that results from our study may provide another example of across strike faults behaving in an out of phase manner, reinforced by two sets of different age controls (Mechernich et al., 2018; Pirazzoli et al., 1994). Whilst the causal explanation of such out of phase behavior remains to be seen, present theories focus on the role of viscous roots (shear zones) at mid- and lower-crustal depths as drivers of brittle fault slip-rate fluctuations through processes of annealing and weakening (Dolan et al., 2007) or differential stress changes (Mildon et al., 2022; Roberts et al., 2024, 2025). More work is needed to investigate the first order controls on across strike out of phase fault behavior because it has implications on (a) the seismic hazard posed by faults in a region and how this can be modeled and, (b) our understanding of crustal rheology, because viscosity is directly related to the strain rate. A change in strain rates between earthquake clusters and anti-clusters implies a change in viscosity which means the strength of the lithosphere may vary through time (e.g., Roberts et al., 2024).

Overall, this paper demonstrates that the timing and magnitudes of slip on crustal-scale faults provided by in situ ^{36}Cl cosmogenic dating of fault scarps can be considered robust, because the implied fault slip history is compatible with the spatial elevations and formation ages of uplifted coastal notches obtained from ^{14}C dating. This agreement of ^{36}Cl and ^{14}C results opens the possibility of more detailed studies of coastal uplift, sea-level and climate histories, and understanding the dynamics of active faulting and continental deformation.

6. Conclusions

In situ ^{36}Cl slip histories on normal faults form the foundation of studies investigating the characteristics of earthquake clustering, the migration of rapid slip pulses (earthquake clusters) on across strike faults and, the role of brittle fault/shear zone stress interactions between neighboring normal faults as a control on the timing and duration of earthquake clusters (e.g., Benedetti et al., 2002; Benedetti et al., 2013; Dawood et al., 2024; Iezzi et al., 2021; Mechernich et al., 2018, 2023; Mildon et al., 2022; Mozafari et al., 2019, 2021; Palumbo et al., 2004; Roberts et al., 2024, 2025; Sgambato et al., 2025; Tesson & Benedetti, 2019; Zreda & Noller, 1998). Our findings show that the spatial patterns of deformed radiocarbon-dated Holocene notches agree with the timing of periods of high slip associated with earthquake clusters and quiescence associated with anti-clusters using the slip histories derived from ^{36}Cl concentrations. These findings suggest that our study may validate ^{36}Cl cosmogenic exposure dating of active normal fault scarps as a method to derive the timing and magnitude of earthquake slip.

The present-day subaerial and submerged elevations of deformed Holocene notches on the north Perachora coastline are explained by a combination of recent (2.0 ± 0.5 ka to the present day) slip on the Pisia fault and high slip rates on the offshore Strava fault between 5.2 ± 0.5 ka to 2.0 ± 0.5 ka. This finding illustrates that across strike (parallel) normal faults have the capacity to induce temporally complex coastal deformation. We emphasize that a combination of geochronological approaches, geomorphological investigations and coseismic earthquake modeling can be used to investigate the interplay between onshore and offshore fault activity and derive estimates of slip rates on offshore faults that lack known deformation rates. Specifically, our modeling and calculations allow us to hypothesize that the Strava fault may slip out of phase with the across-strike Pisia fault. This potential example of out of phase slip behavior on two across-strike faults supports other studies that attest to across-strike faults taking it in turns to accommodate extensional continental deformation (Iezzi et al., 2021; Mildon et al., 2022; Roberts et al., 2024, 2025; Sgambato et al., 2025). We also estimate an in-cluster (5.2 ± 0.5 ka to 2.0 ± 0.5 ka) slip rate on the Strava fault of 3.7–4.9 mm/yr, which should be considered in future seismic hazard assessments.

Conflict of Interest

The authors declare no conflicts of interest relevant to this study.

Data Availability Statement

Calculations of vertical deformation were made using Coulomb software version 3.4 (Toda et al., 2011). We modeled 3D strike-variable fault planes in Coulomb 3.4 using the approach in Mildon et al. (2016), and software in Diercks et al. (2023). The code used to invert for slip histories from ^{36}Cl measurements is from Beck et al. (2018).

Acknowledgments
This work was supported by a Natural Environment Research Council Standard Grant (Grant NE/V012894/1). Original development of the 3D-faults code was supported by NERC PhD Studentship NE/L501700/1 and JSPS Short Term Fellowship PE15776 to Zoe Mildon. Our thanks to the Editor, Anke Friedrich. We are grateful for the Associate Editor's input and comments from two anonymous reviewers which helped to improve the manuscript.

References

Abercrombie, R. E., Main, I. G., Douglas, A., & Burton, P. W. (1995). The nucleation and rupture process of the 1981 Gulf of Corinth earthquakes from deconvolved broad-band data. *Geophysical Journal International*, *120*(2), 393–405. https://doi.org/10.1111/j.1365-246x.1995.tb01827.x

Ambraseys, N. N., & Jackson, J. A. (1990). Seismicity and associated strain of central Greece between 1890 and 1988. *Geophysical Journal International*, *101*(3), 663–708. https://doi.org/10.1111/j.1365-246x.1990.tb05577.x

Antonioli, F., Presti, V. L., Rovere, A., Ferranti, L., Anzidei, M., Furlani, S., et al. (2015). Tidal notches in Mediterranean Sea: A comprehensive analysis. *Quaternary Science Reviews*, *119*, 66–84. https://doi.org/10.1016/j.quascirev.2015.03.016

Armijo, R., Meyer, B. G. C. P., King, G. C. P., Rigo, A., & Papanastassiou, D. (1996). Quaternary evolution of the Corinth rift and its implications for the late Cenozoic evolution of the Aegean. *Geophysical Journal International*, *126*(1), 11–53. https://doi.org/10.1111/j.1365-246x.1996.tb05264.x

Beck, J., Wolfers, S., & Roberts, G. P. (2018). Bayesian earthquake dating and seismic hazard assessment using chlorine-36 measurements (BED v1) [Software]. *Geoscientific Model Development Zenodo*, *11*(11), 4383–4397. https://doi.org/10.5281/zenodo.1402093

Bell, R. E., McNeill, L. C., Bull, J. M., Henstock, T. J., Collier, R. L., & Leeder, M. R. (2009). Fault architecture, basin structure and evolution of the Gulf of Corinth rift, central Greece. *Basin Research*, *21*(6), 824–855. https://doi.org/10.1111/j.1365-2117.2009.00401.x

Benedetti, L., Finkel, R., King, G., Armijo, R., Papanastassiou, D., Ryerson, F. J., et al. (2003). Motion on the Kaparelli fault (Greece) prior to the 1981 earthquake sequence determined from ^{36}Cl cosmogenic dating. *Terra Nova*, *15*(2), 118–124. https://doi.org/10.1046/j.1365-3121.2003.00474.x

Benedetti, L., Finkel, R., Papanastassiou, D., King, G., Armijo, R., Ryerson, F., et al. (2002). Post-glacial slip history of the Sparta fault (Greece) determined by ^{36}Cl Cosmogenic dating: Evidence for non-periodic earthquakes. *Geophysical Research Letters*, *29*(8), 87. https://doi.org/10.1029/2001gl014510

Benedetti, L., Manighetti, I., Gaudemer, Y., Finkel, R., Malavieille, J., Pou, K., et al. (2013). Earthquake synchrony and clustering on Fucino faults (central Italy) as revealed from in situ ^{36}Cl exposure dating. *Journal of Geophysical Research: Solid Earth*, *118*(9), 4948–4974. https://doi.org/10.1002/jgrb.50299

Bennett, R. A., Friedrich, A. M., & Furlong, K. P. (2004). Codependent histories of the San Andreas and San Jacinto fault zones from inversion of fault displacement rates. *Geology*, *32*(11), 961–964. https://doi.org/10.1130/g20806.1

Bornovas, J., Gaitanakis, P., & Spiridopoulos, A. (1984). *Geological map of Greece, 1:50 000, Perachora sheet*. IGME.

Boulton, S. J., & Stewart, I. S. (2015). Holocene coastal notches in the Mediterranean region: Indicators of palaeoseismic clustering? *Geomorphology*, *237*, 29–37. https://doi.org/10.1016/j.geomorph.2013.11.012

Briole, P., Ganas, A., Elias, P., & Dimitrov, D. (2021). The GPS velocity field of the Aegean. New observations, contribution of the earthquakes, crustal blocks model. *Geophysical Journal International*, *226*(1), 468–492. https://doi.org/10.1093/gji/ggab089

Briole, P., Rigo, A., Lyon-Caen, H., Ruegg, J. C., Papazissi, K., Mitsakaki, C., et al. (2000). Active deformation of the Corinth rift, Greece: Results from repeated Global positioning system surveys between 1990 and 1995. *Journal of Geophysical Research*, *105*(B11), 25605–25625. https://doi.org/10.1029/2000jb900148

Charalampakis, M., Lykousis, V., Sakellariou, D., Papatheodorou, G., & Ferentinos, G. (2014). The tectono-sedimentary evolution of the Lechaion Gulf, the south eastern branch of the Corinth Graben, Greece. *Marine Geology*, *351*, 58–75. https://doi.org/10.1016/j.margeo.2014.03.014

Clarke, P. J., Davies, R. R., England, P. C., Parsons, B., Billiris, H., Paradissis, D., et al. (1998). Crustal strain in central Greece from repeated GPS measurements in the interval 1989–1997. *Geophysical Journal International*, *135*(1), 195–214. https://doi.org/10.1046/j.1365-246x.1998.00633.x

Collier, R. E., Pantosti, D., D'Addezio, G., De Martini, P. M., Masana, E., & Sakellariou, D. (1998). Paleoseismicity of the 1981 Corinth earthquake fault: Seismic contribution to extensional strain in central Greece and implications for seismic hazard. *Journal of Geophysical Research*, *103*(B12), 30001–30019. https://doi.org/10.1029/98jb02643

Collier, R. L., Leeder, M. R., Rowe, P. J., & Atkinson, T. C. (1992). Rates of tectonic uplift in the Corinth and Megara basins, Central Greece. *Tectonics*, *11*(6), 1159–1167. https://doi.org/10.1029/92tc01565

Cooper, F. J., Roberts, G. P., & Underwood, C. J. (2007). A comparison of 10^3–10^5 year uplift rates on the South Alkyonides fault, central Greece: Holocene climate stability and the formation of coastal notches. *Geophysical Research Letters*, *34*(14). https://doi.org/10.1029/2007gl030673

Cowie, P. A., Phillips, R. J., Roberts, G. P., McCaffrey, K., Zijerveld, L. J. J., Gregory, L. C., et al. (2017). Orogen-scale uplift in the central Italian Apennines drives episodic behaviour of earthquake faults. *Scientific Reports*, *7*(1), 44858. https://doi.org/10.1038/srep44858

Davies, R., England, P. C., Parsons, B., Billiris, H., Paradissis, D., & Veis, G. (1997). Geodetic strain of Greece in the interval 1892–1992. *Journal of Geophysical Research*, *102*(B11), 24571–24588. https://doi.org/10.1029/97jb01644

Dawood, R., Matmon, A., ASTER Team, & Siman-Tov, S. (2024). Multi-segment earthquake clustering as inferred from ^{36}Cl exposure dating, the Bet Kerem fault system, northern Israel. *Tectonics*, *43*(5), e2023TC007953. https://doi.org/10.1029/2023tc007953

de Gelder, G., Fernández-Blanco, D., Melnick, D., Duclaux, G., Bell, R. E., Jara-Muñoz, J., et al. (2019). Lithospheric flexure and rheology determined by climate cycle markers in the Corinth rift. *Scientific Reports*, *9*(1), 4260. https://doi.org/10.1038/s41598-018-36377-1

Dia, A. N., Cohen, A. S., O'nions, R. K., & Jackson, J. A. (1997). Rates of uplift investigated through ^{230}Th dating in the Gulf of Corinth (Greece). *Chemical Geology*, *138*(3–4), 171–184. https://doi.org/10.1016/s0009-2541(97)00010-7

Diercks, M. L., Mildon, Z. K., Boulton, S. J., Hussain, E., Alçiçek, M. C., Yıldırım, C., & Aykut, T. (2023). Constraining historical earthquake sequences with Coulomb stress models: An example from western Türkiye [Software]. *Journal of Geophysical Research: Solid Earth*, *128*(11). https://doi.org/10.5281/zenodo.7428878

Dolan, J. F., Bowman, D. D., & Sammis, C. G. (2007). Long-range and long-term fault interactions in Southern California. *Geology*, *35*(9), 855–858. https://doi.org/10.1130/g23789a.1

Dolan, J. F., Van Dissen, R. J., Rhodes, E. J., Zinke, R., Hatem, A. E., McGuire, C., et al. (2024). One tune, many tempos: Faults trade off slip in time and space to accommodate relative plate motions. *Earth and Planetary Science Letters*, *625*, 118484. https://doi.org/10.1016/j.epsl.2023.118484

Dunai, T. J. (2010). *Cosmogenic nuclides: Principles, concepts and applications in the Earth surface sciences*. Cambridge University Press.

Evelpidou, N. (2012). Modelling of erosional processes in the Ionian Islands (Greece). *Geomatics, Natural Hazards and Risk*, *3*(4), 293–310. https://doi.org/10.1080/19475705.2011.604798

Evelpidou, N., Ganas, A., Karkani, A., Spyrou, E., & Saitis, G. (2023). Late Quaternary relative sea-level changes and vertical GNSS motions in the Gulf of Corinth: The asymmetric localization of deformation inside an active half-Graben. *Geosciences*, *13*(11), 329. https://doi.org/10.3390/geosciences13110329

Evelpidou, N., Kampolis, I., Pirazzoli, P. A., & Vassilopoulos, A. (2012). Global sea-level rise and the disappearance of tidal notches. *Global and Planetary Change*, *92*, 248–256. https://doi.org/10.1016/j.gloplacha.2012.05.013

Evelpidou, N., Melini, D., Pirazzoli, P. A., & Vassilopoulos, A. (2014). Evidence of repeated late Holocene rapid subsidence in the SE Cyclades (Greece) deduced from submerged notches. *International Journal of Earth Sciences*, *103*(1), 381–395. https://doi.org/10.1007/s00531-013-0942-0

Evelpidou, N., & Pirazzoli, P. A. (2016). Estimation of the intertidal bioerosion rate from a well-dated fossil tidal notch in Greece. *Marine Geology*, *380*, 191–195. https://doi.org/10.1016/j.margeo.2016.04.017

Evelpidou, N., Pirazzoli, P. A., Saliège, J. F., & Vassilopoulos, A. (2011). Submerged notches and doline sediments as evidence for Holocene subsidence. *Continental Shelf Research*, *31*(12), 1273–1281. https://doi.org/10.1016/j.csr.2011.05.002

Evelpidou, N., Vassilopoulos, A., & Pirazzoli, P. A. (2012). Holocene emergence in Euboea Island (Greece). *Marine Geology*, *295*, 14–19. https://doi.org/10.1016/j.margeo.2011.11.010

Faivre, S., Bakran-Petricioli, T., Barešić, J., & Horvatić, D. (2021). Lithophyllum rims as biological markers for constraining palaeoseismic events and relative sea-level variations during the last 3.3 ka on Lopud Island, southern Adriatic, Croatia. *Global and Planetary Change*, *202*, 103517. https://doi.org/10.1016/j.gloplacha.2021.103517

Friedrich, A. M., Wernicke, B. P., Niemi, N. A., Bennett, R. A., & Davis, J. L. (2003). Comparison of geodetic and geologic data from the Wasatch region, Utah, and implications for the spectral character of Earth deformation at periods of 10 to 10 million years. *Journal of Geophysical Research*, *108*(B4). https://doi.org/10.1029/2001jb000682

Ganas, A., Elias, P., Briole, P., Valkaniotis, S., Escartin, J., Tsironi, V., et al. (2021). Co-seismic and post-seismic deformation, field observations and fault model of the 30 October 2020 Mw= 7.0 Samos earthquake, Aegean Sea. *Acta Geophysica*, *69*(3), 999–1024. https://doi.org/10.1007/s11600-021-00599-1

García-Artola, A., Stéphan, P., Cearreta, A., Kopp, R. E., Khan, N. S., & Horton, B. P. (2018). Holocene sea-level database from the Atlantic coast of Europe. *Quaternary Science Reviews*, *196*, 177–192. https://doi.org/10.1016/j.quascirev.2018.07.031

Gauriau, J., & Dolan, J. (2024). Comparison of geodetic slip-deficit and geologic fault slip rates reveals that variability of elastic strain accumulation and release rates on strike-slip faults is controlled by the relative structural complexity of plate-boundary fault systems. *Seismica*, *3*(1). https://doi.org/10.26443/seismica.v3i1.1119

Gelman, A., & Rubin, D. B. (1992). Inference from iterative simulation using multiple sequences. *Statistical Science*, *7*(4), 457–472. https://doi.org/10.1214/ss/1177011136

Gosse, J. C., & Phillips, F. M. (2001). Terrestrial in situ cosmogenic nuclides: Theory and application. *Quaternary Science Reviews*, *20*(14), 1475–1560. https://doi.org/10.1016/s0277-3791(00)00171-2

Hubert, A., King, G., Armijo, R., Meyer, B., & Papanastasiou, D. (1996). Fault re-activation, stress interaction and rupture propagation of the 1981 Corinth earthquake sequence. *Earth and Planetary Science Letters*, *142*(3–4), 573–585. https://doi.org/10.1016/0012-821x(96)00108-2

Iezzi, F., Roberts, G., Faure Walker, J., Papanikolaou, I., Ganas, A., Deligiannakis, G., et al. (2021). Temporal and spatial earthquake clustering revealed through comparison of millennial strain-rates from ^{36}Cl cosmogenic exposure dating and decadal GPS strain-rate. *Scientific Reports*, *11*(1), 23320. https://doi.org/10.1038/s41598-021-02131-3

Jackson, J. A., Gagnepain, J., Houseman, G., King, G. C. P., Papadimitriou, P., Soufleris, C., & Virieux, J. (1982). Seismicity, normal faulting, and the geomorphological development of the Gulf of Corinth (Greece): The Corinth earthquakes of February and March 1981. *Earth and Planetary Science Letters*, *57*(2), 377–397. https://doi.org/10.1016/0012-821x(82)90158-3

Kershaw, S., & Guo, L. (2001). Marine notches in coastal cliffs: Indicators of relative sea-level change, Perachora Peninsula, central Greece. *Marine Geology*, *179*(3–4), 213–228. https://doi.org/10.1016/s0025-3227(01)00218-3

Kershaw, S., & Guo, L. (2003). Pleistocene cyanobacterial mounds in the Perachora Peninsula, Gulf of Corinth, Greece: Structure and applications to interpreting sea-level history and terrace sequences in an unstable tectonic setting. *Palaeogeography, Palaeoclimatology, Palaeoecology*, *193*(3–4), 503–514. https://doi.org/10.1016/s0031-0182(03)00263-3

Khoury, S. G., Tilford, N. R., Chandra, U., & Amick, D. (1983). The effect of multiple events on isoseismal maps of the 1981 earthquakes at the Gulf of Corinth, Greece. *Bulletin of the Seismological Society of America*, *73*(2), 655–660. https://doi.org/10.1785/bssa0730020655

Kim, W. Y., Kulhánek, O., & Meyer, K. (1984). Source processes of the 1981 Gulf of Corinth earthquake sequence from body-wave analysis. *Bulletin of the Seismological Society of America*, *74*(2), 459–477. https://doi.org/10.1785/bssa0740020459

Lambeck, K., Antonioli, F., Purcell, A., & Silenzi, S. (2004). Sea-level change along the Italian coast for the past 10,000 yr. *Quaternary Science Reviews*, *23*(14–15), 1567–1598. https://doi.org/10.1016/j.quascirev.2004.02.009

Lambeck, K., & Purcell, A. (2005). Sea-level change in the Mediterranean Sea since the LGM: Model predictions for tectonically stable areas. *Quaternary Science Reviews*, *24*(18–19), 1969–1988. https://doi.org/10.1016/j.quascirev.2004.06.025

Leeder, M. R., McNeill, L. C., Ll Collier, R. E., Portman, C., Rowe, P. J., Andrews, J. E., & Gawthorpe, R. L. (2003). Corinth rift margin uplift: New evidence from late Quaternary marine shorelines. *Geophysical Research Letters*, *30*(12). https://doi.org/10.1029/2003gl017382

Leeder, M. R., Portman, C., Andrews, J. E., Collier, R. L., Finch, E., Gawthorpe, R. L., et al. (2005). Normal faulting and crustal deformation, Alkyonides Gulf and Perachora peninsula, eastern Gulf of Corinth rift, Greece. *Journal of the Geological Society*, *162*(3), 549–561. https://doi.org/10.1144/0016-764904-075

Manighetti, I., Campillo, M., Bouley, S., & Cotton, F. (2007). Earthquake scaling, fault segmentation, and structural maturity. *Earth and Planetary Science Letters*, *253*(3–4), 429–438. https://doi.org/10.1016/j.epsl.2006.11.004

Mayewski, P. A., Rohling, E. E., Stager, J. C., Karlén, W., Maasch, K. A., Meeker, L. D., et al. (2004). Holocene climate variability. *Quaternary Research*, *62*(3), 243–255. https://doi.org/10.1016/j.yqres.2004.07.001

McNeill, L. C., Cotterill, C. J., Henstock, T. J., Bull, J. M., Stefatos, A., Collier, R. L., et al. (2005). Active faulting within the offshore western Gulf of Corinth, Greece: Implications for models of continental rift deformation. *Geology*, *33*(4), 241–244. https://doi.org/10.1130/g21127.1

Mechernich, S., Reicherter, K., Deligiannakis, G., & Papanikolaou, I. (2023). Tectonic geomorphology of active faults in Eastern Crete (Greece) with slip rates and earthquake history from cosmogenic ^{36}Cl dating of the Lastros and Orno faults. *Quaternary International*, *651*, 77–91. https://doi.org/10.1016/j.quaint.2022.04.007

Mechernich, S., Schneiderwind, S., Mason, J., Papanikolaou, I. D., Deligiannakis, G., Pallikarakis, A., et al. (2018). The seismic history of the Pisia fault (eastern Corinth rift, Greece) from fault plane weathering features and cosmogenic ^{36}Cl dating. *Journal of Geophysical Research: Solid Earth*, *123*(5), 4266–4284. https://doi.org/10.1029/2017jb014600

Meschis, M., Roberts, G. P., Robertson, J., Mildon, Z. K., Sahy, D., Goswami, R., et al. (2022). Out of phase quaternary uplift-rate changes reveal normal fault interaction, implied by deformed marine palaeoshorelines. *Geomorphology*, *416*, 108432. https://doi.org/10.1016/j.geomorph.2022.108432

Mildon, Z. K., Diercks, M., Roberts, G. P., Faure Walker, J. P., Ganas, A., Papanikolaou, I., et al. (2024). Transient aseismic vertical deformation across the steeply-dipping Pisia-Skinos normal fault (Gulf of Corinth, Greece). *Tectonics*, *43*(8), e2024TC008276. https://doi.org/10.1029/2024tc008276

Mildon, Z. K., Roberts, G. P., Faure Walker, J. P., Beck, J., Papanikolaou, I., Michetti, A. M., et al. (2022). Surface faulting earthquake clustering controlled by fault and shear-zone interactions. *Nature Communications*, *13*(1), 7126. https://doi.org/10.1038/s41467-022-34821-5

Mildon, Z. K., Toda, S., Faure Walker, J. P., & Roberts, G. P. (2016). Evaluating models of Coulomb stress transfer: Is variable fault geometry important? *Geophysical Research Letters*, *43*(24), 12–407. https://doi.org/10.1002/2016gl071128

Mitchell, S., Roberts, G. P., Walker, J. P. F., Iezzi, F., Sgambato, C., Robertson, J., et al. (2024). The relationship between kinematics and fault geometry for surface coseismic ruptures on across-strike faults: New observations of slip vectors and displacements along the Pisia and Skinos faults from the 1981 Eastern Gulf of Corinth, Greece earthquakes. *Journal of Structural Geology*, *182*, 105117. https://doi.org/10.1016/j.jsg.2024.105117

Morewood, N. C., & Roberts, G. P. (1997). Geometry, kinematics and rates of deformation in a normal fault segment boundary, central Greece. *Geophysical Research Letters*, *24*(23), 3081–3084. https://doi.org/10.1029/97gl03100

Morewood, N. C., & Roberts, G. P. (1999). Lateral propagation of the surface trace of the South Alkyonides normal fault segment, central Greece: Its impact on models of fault growth and displacement–length relationships. *Journal of Structural Geology*, *21*(6), 635–652. https://doi.org/10.1016/s0191-8141(99)00049-8

Morewood, N. C., & Roberts, G. P. (2001). Comparison of surface slip and focal mechanism slip data along normal faults: An example from the eastern Gulf of Corinth, Greece. *Journal of Structural Geology*, *23*(2–3), 473–487. https://doi.org/10.1016/s0191-8141(00)00126-7

Morewood, N. C., & Roberts, G. P. (2002). Surface observations of active normal fault propagation: Implications for growth. *Journal of the Geological Society*, *159*(3), 263–272. https://doi.org/10.1144/0016-764901-046

Mozafari, N., Özkaymak, Ç., Tikhomirov, D., Ivy-Ochs, S., Alfimov, V., Sözbilir, H., et al. (2021). Seismic activity of the Manisa Fault zone in Western Turkey constrained by cosmogenic ^{36}Cl dating. *Geosciences*, *11*(11), 451. https://doi.org/10.3390/geosciences11110451

Mozafari, N., Sümer, Ö., Tikhomirov, D., Ivy-Ochs, S., Alfimov, V., Vockenhuber, C., et al. (2019). Holocene seismic activity of the Priene-Sazlı Fault revealed by cosmogenic ^{36}Cl, western Anatolia, Turkey. *Turkish Journal of Earth Sciences*, *28*(3), 410–437. https://doi.org/10.3906/yer-1810-6

Nixon, C. W., McNeill, L. C., Bull, J. M., Bell, R. E., Gawthorpe, R. L., Henstock, T. J., et al. (2016). Rapid spatiotemporal variations in rift structure during development of the Corinth rift, Central Greece. *Tectonics*, *35*(5), 1225–1248. https://doi.org/10.1002/2015tc004026

Palumbo, L., Benedetti, L., Bourlès, D., Cinque, A., & Finkel, R. (2004). Slip history of the Magnola fault (Apennines, Central Italy) from ^{36}Cl surface exposure dating: Evidence for strong earthquakes over the Holocene. *Earth and Planetary Science Letters*, *225*(1–2), 163–176. https://doi.org/10.1016/j.epsl.2004.06.012

Papanikolaou, I. D., Foumelis, M., Parcharidis, I., Lekkas, E. L., & Fountoulis, I. G. (2010). Deformation pattern of the 6 and 7 April 2009, M W= 6.3 and M W= 5.6 earthquakes in L'Aquila (Central Italy) revealed by ground and space based observations. *Natural Hazards and Earth System Sciences*, *10*(1), 73–87.

Papatheodorou, G., & Ferentinos, G. (1993). Sedimentation processes and basin-filling depositional architecture in an active asymmetric Graben: Strava Graben, Gulf of Corinth, Greece. *Basin Research*, *5*(4), 235–253. https://doi.org/10.1111/j.1365-2117.1993.tb00069.x

Papazachos, B. C., Comninakis, P. E., Papadimitriou, E. E., & Scordilis, E. M. (1984). Properties of the February–March 1981 seismic sequence in the Alkyonides gulf of central Greece. *Annals of Geophysics*, *2*(5), 537–544.

Pirazzoli, P. A. (1986). Secular trends of Relative Sea-Level (RSL) changes indicated by tide-gauge records. *Journal of Coastal Research*, 1–26. https://www.jstor.org/stable/44863318

Pirazzoli, P. A. (1991). World atlas of Holocene sea-level changes.

Pirazzoli, P. A., & Evelpidou, N. (2013). Tidal notches: A sea-level indicator of uncertain archival trustworthiness. *Palaeogeography, Palaeoclimatology, Palaeoecology*, *369*, 377–384. https://doi.org/10.1016/j.palaeo.2012.11.004

Pirazzoli, P. A., Laborel, J., & Stiros, S. C. (1996). Earthquake clustering in the Eastern Mediterranean during historical times. *Journal of Geophysical Research*, *101*(B3), 6083–6097. https://doi.org/10.1029/95jb00914

Pirazzoli, P. A., Stiros, S. C., Arnold, M., Laborel, J., Laborel-Deguen, F., & Papageorgiou, S. (1994). Episodic uplift deduced from Holocene shorelines in the Perachora Peninsula, Corinth area, Greece. *Tectonophysics*, *229*(3–4), 201–209. https://doi.org/10.1016/0040-1951(94)90029-9

Roberts, G. P. (1996a). Noncharacteristic normal faulting surface ruptures from the Gulf of Corinth, Greece. *Journal of Geophysical Research*, *101*(B11), 25255–25267. https://doi.org/10.1029/96jb02119

Roberts, G. P. (1996b). Variation in fault-slip directions along active and segmented normal fault systems. *Journal of Structural Geology*, *18*(6), 835–845. https://doi.org/10.1016/s0191-8141(96)80016-2

Roberts, G. P., & Ganas, A. (2000). Fault-slip directions in central and southern Greece measured from striated and corrugated fault planes: Comparison with focal mechanism and geodetic data. *Journal of Geophysical Research*, *105*(B10), 23443–23462. https://doi.org/10.1029/1999jb900440

Roberts, G. P., Houghton, S. L., Underwood, C., Papanikolaou, I., Cowie, P. A., van Calsteren, P., et al. (2009). Localization of quaternary slip rates in an active rift in 105 years: An example from central Greece constrained by ^{234}U–^{230}Th coral dates from uplifted paleoshorelines. *Journal of Geophysical Research*, *114*(B10). https://doi.org/10.1029/2008jb005818

Roberts, G. P., Iezzi, F., Sgambato, C., Robertson, J., Beck, J., Mildon, Z. K., et al. (2025). Characteristics and modelling of slip-rate variability and temporal earthquake clustering across a distributed network of active normal faults constrained by in situ ^{36}Cl cosmogenic dating of fault scarp exhumation, central Italy. *Journal of Structural Geology*, *195*, 105391. https://doi.org/10.1016/j.jsg.2025.105391

Roberts, G. P., Sgambato, C., Mildon, Z. K., Iezzi, F., Beck, J., Robertson, J., et al. (2024). Spatial migration of temporal earthquake clusters driven by the transfer of differential stress between neighbouring fault/shear-zone structures. *Journal of Structural Geology*, *181*, 105096. https://doi.org/10.1016/j.jsg.2024.105096

Robertson, J., Roberts, G. P., Iezzi, F., Meschis, M., Gheorghiu, D. M., Sahy, D., et al. (2020). Distributed normal faulting in the tip zone of the South Alkyonides fault system, Gulf of Corinth, constrained using ^{36}Cl exposure dating of late-quaternary wave-cut platforms. *Journal of Structural Geology*, *136*, 104063. https://doi.org/10.1016/j.jsg.2020.104063

Rust, D., & Kershaw, S. (2000). Holocene tectonic uplift patterns in northeastern Sicily: Evidence from marine notches in coastal outcrops. *Marine Geology*, *167*(1–2), 105–126. https://doi.org/10.1016/s0025-3227(00)00019-0

Sakellariou, D., Lykousis, V., Alexandri, S., Kaberi, H., Rousakis, G., Nomikou, P., et al. (2007). Faulting, seismic-stratigraphic architecture and late quaternary evolution of the Gulf of Alkyonides basin–East Gulf of Corinth, Central Greece. *Basin Research*, *19*(2), 273–295. https://doi.org/10.1111/j.1365-2117.2007.00322.x

Schlagenhauf, A., Gaudemer, Y., Benedetti, L., Manighetti, I., Palumbo, L., Schimmelpfennig, I., et al. (2010). Using in situ Chlorine-36 Cosmonuclide to recover past earthquake histories on limestone normal fault scarps: A reappraisal of methodology and interpretations. *Geophysical Journal International*, *182*(1), 36–72. https://doi.org/10.1111/j.1365-246x.2010.04622.x

Schneiderwind, S., Boulton, S. J., Papanikolaou, I., Kázmér, M., & Reicherter, K. (2017). Numerical modeling of tidal notch sequences on rocky coasts of the Mediterranean Basin. *Journal of Geophysical Research: Earth Surface*, *122*(5), 1154–1181. https://doi.org/10.1002/2016jf004132

Schneiderwind, S., Boulton, S. J., Papanikolaou, I., & Reicherter, K. (2017). Innovative tidal notch detection using TLS and fuzzy logic: Implications for Palaeo-shorelines from compressional (Crete) and extensional (Gulf of Corinth) tectonic settings. *Geomorphology*, *283*, 189–200. https://doi.org/10.1016/j.geomorph.2017.01.028

Sgambato, C., Roberts, G. P., Iezzi, F., Faure Walker, J. P., Beck, J., Mildon, Z. K., et al. (2025). Millennial slip-rates variability of along-strike active faults in the Italian Southern Apennines revealed by cosmogenic ^{36}Cl dating of fault scarps. *Tectonics*, *44*(3), e2024TC008529. https://doi.org/10.1029/2024tc008529

Stefatos, A., Papatheodorou, G., Ferentinos, G., Leeder, M., & Collier, R. (2002). Seismic reflection imaging of active offshore faults in the Gulf of Corinth: Their seismotectonic significance. *Basin Research*, *14*(4), 487–502. https://doi.org/10.1046/j.1365-2117.2002.00176.x

Stein, R. S., & Barrientos, S. E. (1985). Planar high-angle faulting in the basin and range: Geodetic analysis of the 1983 Borah Peak, Idaho, earthquake. *Journal of Geophysical Research*, *90*(B13), 11355–11366. https://doi.org/10.1029/jb090ib13p11355

Stewart, I., & Vita-Finzi, C. (1996). Coastal uplift on active normal faults: The Eliki fault, Greece. *Geophysical Research Letters*, *23*(14), 1853–1856. https://doi.org/10.1029/96gl01595

Stiros, S. & Pirazzoli, P. A. (Eds.) (1998). *Late Quaternary coastal changes in the Gulf of Corinth, Greece: Tectonics, earthquakes, archaeology*. Geodesy Laboratory, Department of Civil Engineering, Patras University.

Taylor, B., Weiss, J. R., Goodliffe, A. M., Sachpazi, M., Laigle, M., & Hirn, A. (2011). The structures, stratigraphy and evolution of the Gulf of Corinth rift, Greece. *Geophysical Journal International*, *185*(3), 1189–1219. https://doi.org/10.1111/j.1365-246x.2011.05014.x

Taymaz, T., Jackson, J., & McKenzie, D. (1991). Active tectonics of the north and central Aegean Sea. *Geophysical Journal International*, *106*(2), 433–490. https://doi.org/10.1111/j.1365-246x.1991.tb03906.x

Tesson, J., & Benedetti, L. (2019). Seismic history from in situ ^{36}Cl cosmogenic nuclide data on limestone fault scarps using Bayesian reversible jump Markov chain Monte Carlo. *Quaternary Geochronology*, *52*, 1–20. https://doi.org/10.1016/j.quageo.2019.02.004

Tikhomirov, D., Amiri, N. M., Ivy-Ochs, S., Alfimov, V., Vockenhuber, C., & Akçar, N. (2019). Fault scarp dating Tool-a MATLAB code for fault scarp dating using in-situ chlorine-36 supplemented with datasets of Yavansu and Kalafat faults. *Data in Brief*, *26*, 104476. https://doi.org/10.1016/j.dib.2019.104476

Toda, S., Stein, R. S., Sevilgen, V., & Lin, J. (2011). Coulomb 3.3 graphic-rich deformation and stress-change software for earthquake, tectonic, and volcano research and teaching—user guide [Software]. *US Geological Survey open-file report*, *1060*. Retrieved from https://pubs.usgs.gov/of/2011/1060/

Trenhaile, A. S. (2015). Coastal notches: Their morphology, formation, and function. *Earth-Science Reviews*, *150*, 285–304. https://doi.org/10.1016/j.earscirev.2015.08.003

Tsimplis, M. N. (1994). Tidal oscillations in the Aegean and Ionian Seas. *Estuarine, Coastal and Shelf Science*, *39*(2), 201–208. https://doi.org/10.1006/ecss.1994.1058

Vacchi, M., Marriner, N., Morhange, C., Spada, G., Fontana, A., & Rovere, A. (2016). Multiproxy assessment of Holocene relative sea-level changes in the western Mediterranean: Sea-level variability and improvements in the definition of the isostatic signal. *Earth-Science Reviews*, *155*, 172–197. https://doi.org/10.1016/j.earscirev.2016.02.002

Vita-Finzi, C., & King, G. C. P. (1985). The seismicity, geomorphology and structural evolution of the Corinth area of Greece. *Philosophical Transactions of the Royal Society of London—Series A: Mathematical and Physical Sciences*, *314*(1530), 379–407.

Wells, D. L., & Coppersmith, K. J. (1994). New empirical relationships among magnitude, rupture length, rupture width, rupture area, and surface displacement. *Bulletin of the Seismological Society of America*, *84*(4), 974–1002. https://doi.org/10.1785/bssa0840040974
Wesnousky, S. G. (2008). Displacement and geometrical characteristics of earthquake surface ruptures: Issues and implications for seismic-hazard analysis and the process of earthquake rupture. *Bulletin of the Seismological Society of America*, *98*(4), 1609–1632. https://doi.org/10.1785/0120070111
Zreda, M., & Noller, J. S. (1998). Ages of prehistoric earthquakes revealed by cosmogenic chlorine-36 in a bedrock fault scarp at Hebgen Lake. *Science*, *282*(5391), 1097–1099. https://doi.org/10.1126/science.282.5391.1097

References From the Supporting Information

Stone, J. O. (2000). Air pressure and cosmogenic isotope production. *Journal of Geophysical Research*, *105*(B10), 23753–23759. https://doi.org/10.1029/2000jb900181